AERODYNAMIC HEATING OF STUDENT ROCKET PROJECT-5 SOUNDING ROCKET

By

Venkata Mudunuri

RECOMMENDED:

Joseph S. Hawkins
Dr. Joseph Hawkins

Debendra K Das
Dr. Debendra K Das

Dr. Douglas Goering, Advisory Committee Chair

Chair, Department of Mechanical Engineering

APPROVED:

John Aspnes
Dean, College of Engineering and Mines

Susan M Henrichs
Dean of the Graduate School

April 26, 2005
Date

AERODYNAMIC HEATING OF THE STUDENT ROCKET PROJECT-5 SOUNDING ROCKET

A

Thesis

Presented to the Faculty

of the University of Alaska Fairbanks

in Partial Fulfillment of the Requirements

for the Degree of

Master of Science

By

Venkata Mudunuri, B.E

Fairbanks, Alaska

May 2005

ABSTRACT

This thesis deals with the calculation of the flow properties and heat transfer around the rocket nose cone for Student Rocket Project-5 (SRP-5). Governing differential equations are presented for this purpose, giving the fundamental relations between the skin temperature and flight history. The determination of all the required parameters in the equations is discussed, and the Runge-Kutta numerical method of integration is used to obtain the solution. A model to implement the above equations to predict skin temperature for the given trajectory was built in SIMULINK®. Individual sub-systems of the SIMULINK® model are used to calculate local free-stream values, Reynolds number, heat absorption capacity and skin friction coefficient. The SIMULINK® model was used to predict the variation of the skin temperature for the SRP-5 flight trajectory. The simulation results also show comparisons of the different subsystem outputs with data provided by the contractor for the NASA Sounding Rocket Contract (NSROC).

Table of Contents

List of Figures

List of Tables

List of Appendices

Acknowledgements

I would like to gratefully thank my advisor Dr. Douglas Goering for giving me an opportunity to work on this project. I express my sincere thanks for his time and patience along with his guidance. It has been a very good experience working under him and I have learned a lot from him. He has supported me during the course of my Masters studies with the financial assistance of the Alaska Space Grant Project.

My graduate committee members Dr. Debendra Das and Dr. Joseph Hawkins have been helpful in providing valuable suggestions when needed, and I am thankful to them.

Finally, I am grateful to my family and friends who have always been my support

Nomenclature

Q_{local}	Local rate of heat transfer at the surface element ΔA (Btu/sec)
q_a	Aerodynamic heat transfer rate (Btu/sec)
q_r	Heat transfer rate loss due to radiation (Btu/sec)
ΔA	Local element of the surface area (ft^2)
c	Specific heat of the skin material(Btu/lb ^oR)
t	Time (sec)
t_s	Skin thickness (ft)
w	Specific weight of the skin material (lb/ft^3)
h	Film coefficient of the heat transfer (Btu/sec-ft^2-^oR)
T_{aw}	Adiabatic wall temperature (^oR)
T_w	Wall temperature (^oR)
ε	Emissivity of the surface
σ	Stefan-Boltzmann radiation constant
G	Heat absorption capacity of the skin (Btu/ft^2-^oR)
c_{h_∞}	Stanton number
c_p	Specific heat at constant pressure ($ft^2/^oR$-sec^2)
ρ_∞	Local free-stream density ($slugs/ft^3$)
V_∞	Local free-stream velocity (ft/sec)
J	Mechanical equivalent of heat (ft-lb/Btu)
a_∞	Local free-stream speed of sound (ft/sec)
M_∞	Local free-stream Mach number
q	Heat flux (Btu/sec)
k	Coefficient of thermal conductivity (ft^2-lb/slug ^oR)
T_{0_∞}	Free-stream stagnation temperature (^oR)

T_∞	Local free-stream temperature ($^\circ$R)
R	Recovery factor (dimensionless)
c_{f_∞}	Local skin friction coefficient based on local free-stream properties
Pr	Prandtl number
a	Speed of sound
M	Mach number, $\overline{V}/\overline{a}$
u	Non-dimensional velocity along conical ray line in spherical coordinate system, $\overline{u}/\overline{V_l}$
v	Non-dimensional velocity normal to conical ray line in spherical system, $\overline{v}/\overline{V_l}$
γ	Ratio of specific heats, c_p/c_v
θ	Conical ray angle, from cone axis
s	Denotes values, at cone surface

1 Introduction

1.1 Introduction

As actual and proposed speed and altitude of flight increases, the problem of maintaining the temperature of the internal structure of high-speed vehicles within permissible values becomes increasingly difficult. Due to aerodynamic heating, the internal temperatures of an aircraft traveling through the atmosphere at high Mach number may become excessive unless a sufficient amount of cooling is supplied. As an example of one of the difficulties caused by aerodynamic heating, it is known that some German A-4 missiles experienced sufficient internal heating to cause explosion of the fuel tanks prior to impact.

In attempting to solve the thermal problem, it is first necessary to determine the rate at which heat enters the surface, and second, to provide some means which will prevent the heat from becoming excessive in the internal structure of the vehicle. The problem of determining the theoretical heat transfer characteristics dates back to the work of Pohlhausan [3] and Crocco [4]. In 1935 and again in 1938, Von Karman treated the subject of heat transfer for laminar boundary layers [6], [7]. The works by Huston, Warfield and Stone [8], by Van Driest [2], and by Truitt [1] have all extended the knowledge of heat transfer characteristics for both laminar and turbulent boundary layers. The method presented in this thesis for determining the skin temperature is based mainly on the procedure given in the textbook *Fundaments of Aerodynamic Heating* by Triutt [1].

In order to understand the fundamentals of aerodynamic heating, it is first necessary to introduce some fundamental concepts. As its name implies, aerodynamic heating is the heating of an object as a result of the flow of air at high speed about that

object. Friction between the fluid filaments as they stream along the body and compression at and near the stagnation regions of forward surfaces convert the kinetic energy of motion into heat within a thin layer of air surrounding the body. The temperature of this layer increases with the square of the speed so that, already at a Mach Number of 5, the boundary layer temperature attains a value of approximately 3000° R. Since this temperature is concentrated in the air at the surface of the aircraft, heat will flow readily from the boundary layer of the aircraft, the ease with which it flows increasing also with the speed. Therefore, the problem of aerodynamic heating tends to increase in severity as the speed increases. This fact is aptly pointed out in the following quotation from reference [2].

"Because of the increase of the heat transfer with speed, it appears that a "thermal barrier" exists much as it appeared in the past that a "sonic barrier" existed. The problems differ somewhat in that the sonic barrier existed over a narrow band of Mach number, whereas thermal barrier does not occur over a limited range of Mach number but rather tends to increase in severity as the Mach number is increased."

While, as in the case of the sonic barrier, proper design can alleviate some of the problems arising from the thermal barrier, it is obvious that as the flight speeds become very large (say, of the order of Mach numbers of 15 and greater), the surface temperatures will become very high under any design condition. Thus, it appears that the surfaces of high-speed vehicles will have to be made of materials, such as ceramics, which can withstand the high temperatures to which they may be subjected.

Assuming that the surface temperature will be very high, the problem arises of keeping the temperature of the internal structure from becoming excessive. This problem has several possible solutions. Certainly, for flights of long duration at very high speeds, some form of internal cooling will be required. However, since weight is always of prime importance in the design of any aircraft, the weight of a cooling system, capable of

handling the high temperatures encountered at flight speeds of Mach numbers of 15 or grater, may prove to be excessive.

With this in mind, it was suggested by Dr. J. F. Vandrey, Advanced Design Section, The Martin Company, that heat insulation should be used to prevent a portion of the heat from reaching the internal structure of the vehicle. It is expected that, while this will not eliminate the need for internal cooling, it will make possible the use of a much smaller, and thus lighter, cooling system [5].

1.2 Scope of Study

The goal of this thesis is to develop a model that can be used to determine the skin temperatures around the rocket nose cone for the SRP-5 sounding rocket. In this thesis, SIMULINK® is used to model and simulate the procedure given in Truitt [1]. Chapter 2 deals with the basic concepts of aerodynamic heating. It also shows how we derive the governing equation for determining the skin temperature. Chapter 3 deals with calculation of different parameters required for the simulation. Chapter 4 deals with the modeling of the governing equation in SIMULINK®. Chapter 5 deals with the changes made in the model in order to solve the example problem. In Chapter 6, the simulation results of the example problem and the SRP-5 are given. Chapter 7 provides a summary of the present work and suggests future research and modifications.

2 Governing Equations

2.1 Introduction

Aerodynamic heating is the heating of an object as a result of flow of air at high speed about that object. Friction between the fluid filaments while they stream along the body and compression at and near the stagnation regions of forward surfaces convert the kinetic energy of motion into heat within a thin layer of air which blankets the body. Such a region is shown in Figure 2.1 . The temperature of this layer increases with the square of the speed so that, at a Mach number of 3, the boundary-layer temperature attains a value of 600°F. Since this temperature is concentrated in the air at the surface of the aircraft, heat will flow readily from the boundary layer to the aircraft, the ease with which it flows increasing also with speed. Because of the increase of heat transfer with speed, it appears that a "thermal barrier" exists much as it appeared in the past that a "sonic barrier" existed [2].

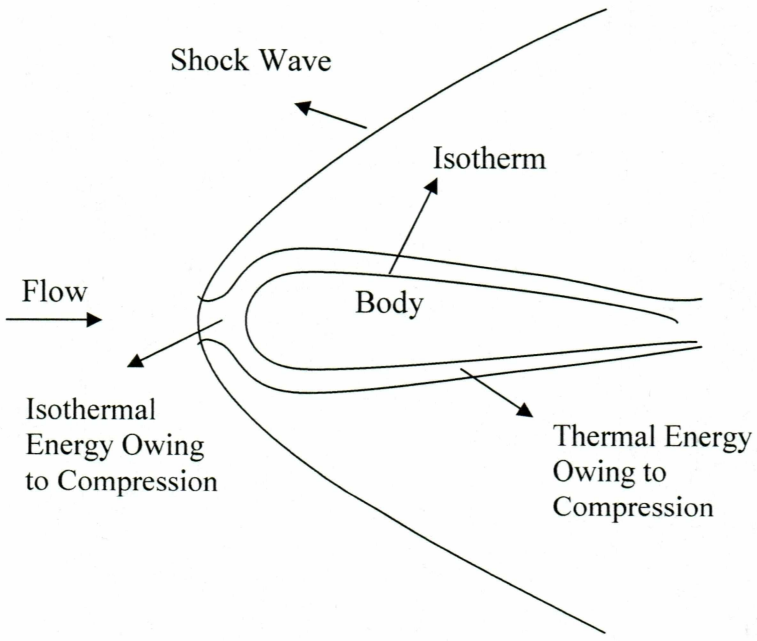

Figure 2.1 Hot region covering body at supersonic speed [2].

However, like the sonic (drag) barrier, which was eventually hurdled by informed design practices, it is believed that the thermal barrier can also be overcome by realistic and proper engineering design. The problems differ somewhat in that the drag barrier existed over a narrow band of Mach numbers, whereas the thermal barrier does not occur over a limited range of Mach numbers, but rather tends to increase in severity as Mach number increases. In attempting to solve the thermal problem, the first question that arises is: What is the rate at which heat enters the surface of a high-speed vehicle? Subsequent questions are: Where does the heat go? What happens when the heat gets there? How can the designer live with it?

2.2 Basic Heat Transfer Equation

For practical aerodynamic heating problems, the local rate of heat transfer into a skin surface element (Q_{local}) is equal to the local aerodynamic heat transfer rate (q_a) at the surface element, minus the radiative heat-transfer (q_r) from the surface element (Neglecting the equipment heat release rate (q_e) and the heat transfer rate into the surface element (q_s), due to the solar radiation. It is given by Eq. 2.1.

$$Q_{local} = q_a - q_r \tag{2.1}$$

The local rate of heat transfer at the surface element ΔA, the aerodynamic heat transfer rate and the heat lost by radiation from the elemental surface area ΔA are given by Eqs. 2.2, 2.3 and 2.4.

$$Q_{local} = \Delta A c t_s w \left(\frac{dT_w}{dt} \right) \tag{2.2}$$

$$q_a = \Delta A h \left(T_{aw} - T_w \right) \tag{2.3}$$

$$q_r = \Delta A \varepsilon \sigma T_w^4 \tag{2.4}$$

Substituting Eqs. 2.2, 2.3 and 2.4 in 2.1 and rearranging the terms, we get:

$$\frac{dT_w}{dt} = \frac{h}{G}(T_{aw} - T_w) - \frac{\varepsilon\sigma T_w^4}{G} \qquad \textbf{2.5}$$

where,

$G = ct_s w$ is the heat absorption capacity of the skin.

The aerodynamic heat transfer, in units of ft^2-^oR/sec per unit area is given by:

$$\frac{q_a}{G} = \frac{h(T_{aw} - T_w)}{G}. \qquad \textbf{2.6}$$

Using the Reynolds analogy between friction and heat transfer, we can write the heat transfer coefficient in terms of the Stanton number as:

$$h = c_{h_\infty} c_p \rho_\infty V_\infty. \qquad \textbf{2.7}$$

Substituting the value of heat transfer coefficient in Eq. 2.6 with 2.7 and replacing the free stream velocity with local free-stream Mach number, we get:

$$\frac{q_a}{G} = \frac{1}{JG} c_{h_\infty} c_p \rho_\infty a_\infty M_\infty (T_{aw} - T_w). \qquad \textbf{2.8}$$

The action of friction in a boundary-layer is always, to a certain extent, affected by heat transfer between fluid layers within the boundary layer. Viscous stresses within the boundary layer do shear work on the fluid particles. This work due to shearing tends

to alter the temperature of fluid particles. These variations in temperature lead to heat conduction and also produce changes in density and viscosity. Since the velocity distribution in the boundary layer depends on the shear stress distribution, as well as on the viscosity and density distribution, it follows that the skin friction is controlled in part by heat transfer within the boundary layer.

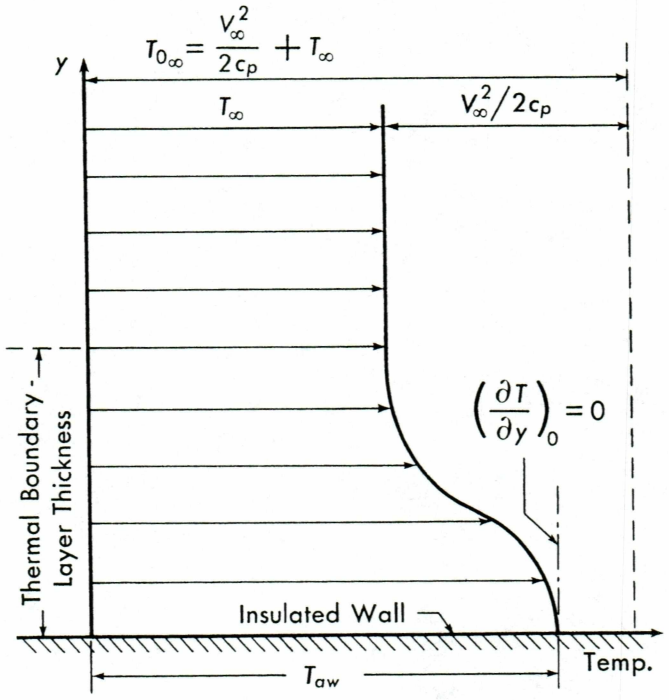

Figure 2.2 Thermal boundary-layer temperature distribution near insulated wall [1].

If we consider a high-speed boundary-layer flow next to a flat wall which is insulated against heat transfer, the outer layer of fluid does viscous shearing work on the inner layers. This causes the internal energy and temperature of the fluid in the inner layers to rise. If there is no heat conduction at all, the inner layers and the wall would become progressively hotter. On the other hand, the temperature gradient caused by the viscous shearing work leads to a conduction of heat away from the wall, which ultimately counterbalances the effect of the shearing work. The resulting steady-state temperature

distribution is shown in Figure 2.2. The adiabatic wall temperature T_{aw} is greater than the free-steam temperature T_{∞}. The temperature gradient is zero at the wall. The Fourier equation for heat conduction in the y-direction is:

$$q = -k\frac{\partial T}{\partial y}. \qquad \textbf{2.9}$$

It is important to note that the adiabatic wall temperature is always less than the free-stream stagnation temperature $T_{w_{\infty}}$. This condition is in contrast to what one may expect from the well-known temperature Mach number relation:

$$\frac{T_1}{T_2} = \frac{1+[(\gamma-1)/2]M_2^2}{1+[(\gamma-1)/2]M_1^2}. \qquad \textbf{2.10}$$

Now if we substitute $T_1 = T_{0_{\infty}}$, $T_2 = T_{\infty}$, $M_1 = 0$ and $M_2 = M_{\infty}$, then we have:

$$T_{0_{\infty}} = T_{\infty}\left(1+\frac{\gamma-1}{2}M_{\infty}^2\right). \qquad \textbf{2.11}$$

$T_{0_{\infty}}$ is the value of the temperature where the velocity is zero. On the other hand, in continuum flow the velocity at the wall is zero, but as already stated, the adiabatic wall temperature is always less than the free-stream stagnation temperature. Therefore, for practical computations, it is convenient to define a quantity known as the recovery factor, which is the measure of the fraction of the local free-stream dynamic-temperature rise recovered at the wall.

$$T_{aw} = T_\infty \left(1 + R\frac{\gamma - 1}{2} M_\infty^2\right) \qquad \textbf{2.12}$$

Using the simple energy equation $\frac{V_\infty^2}{2} + c_p T_\infty = c_p T_{0_\infty}$, the recovery factor can be written as:

$$R = \frac{T_{aw} - T_\infty}{V_\infty^2 / 2c_p} = \frac{T_{aw} - T_\infty}{T_{0_\infty} - T_\infty} = \frac{2}{(\gamma - 1)M_\infty^2}\left(\frac{T_{aw}}{T_\infty} - 1\right). \qquad \textbf{2.13}$$

By using the Reynolds analogy, the Stanton number is related to the local skin-friction coefficient by Eq. 2.14.

$$c_{h_\infty} = \frac{c_{f_\infty}}{2} \mathrm{Pr}^{-(2/3)} \qquad \textbf{2.14}$$

It is obvious that if the entire plate is adiabatic, energy considerations dictate that the mean stagnation temperature with respect to the mass flow must be equal to the free-stream stagnation temperature T_{0_∞}. Since the wall temperature is less than T_{0_∞}, it follows that the distribution of stagnation temperature within the boundary layer must be of the form shown in Figure 2.3, with some portion of the boundary layer having a stagnation temperature greater than T_{0_∞}.

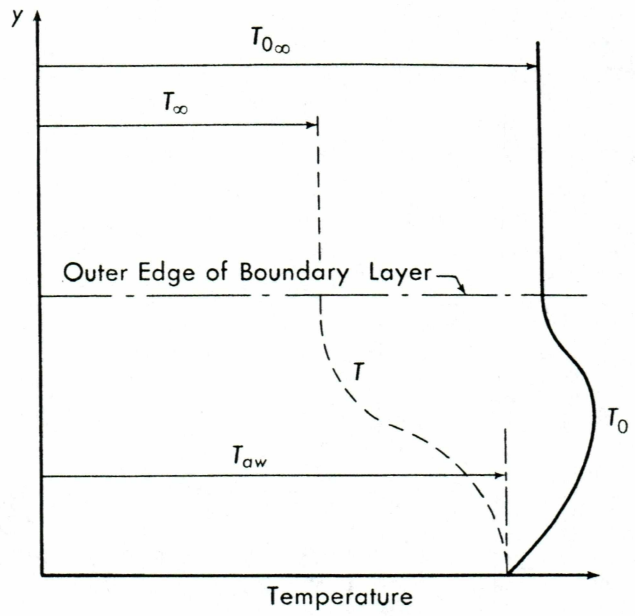

Figure 2.3 Distribution of temperature and stagnation temperature near insulated wall [1].

2.3 Laminar Flow

A great number of solutions of the differential equations for the laminar boundary layer have been worked out and are available to give information for a wide range of conditions, including very high Mach number and large temperature differences. In general, the theoretical results give satisfactory agreement with experiment, and thus in the laminar range reliable predications can be obtained from theoretical calculations.

For the case of laminar flow, the recovery factor varies almost exactly as the square root of the Prandtl number. It is also found that the Prandtl number is also almost independent of Mach number. It has been confirmed that the rule $R = \sqrt{\Pr}$ is accurate when the variation of viscosity through the boundary layer is accounted for.

$$T_{aw} = T_\infty \left(1 + (\Pr)^{1/2} \frac{\gamma - 1}{2} M_\infty^2 \right) \qquad \textbf{2.15}$$

Multiplying equation 2.8 by unity in the form of:

$$\left(2V_\infty^2 / 2V_\infty^2\right)\left(T_{aw} - T_\infty\right)/\left(T_{aw} - T_\infty\right). \qquad \textbf{2.16}$$

we get:

$$\frac{q_a}{G} = \frac{c_{h_\infty}}{JG}\frac{\rho_\infty V_\infty^3}{2}\left(\frac{T_{aw} - T_w}{T_{aw} - T_\infty}\right)\frac{T_{aw} - T_\infty}{\left(V_\infty^2/2c_p\right)}. \qquad \textbf{2.17}$$

Substituting Eqs. 2.13 and 2.14 in 2.17, we get:

$$\frac{q_a}{G} = \frac{1}{JG}\left[\frac{\mathrm{Pr}^{-(1/6)}}{2}\left(\frac{T_{aw} - T_\infty}{T_{aw} - T_\infty}\right)\right]c_{f_\infty}\left(\frac{\rho_\infty a_\infty^3}{2}\right)M_\infty^3. \qquad \textbf{2.18}$$

The governing differential equation for the skin temperature in laminar flow may now be obtained by substituting Eq. 2.18 into 2.5.

$$\frac{dT_w}{dt} = \frac{1}{JG}\left[\frac{1}{2}\mathrm{Pr}^{-(2/3)}\left(\frac{T_{aw} - T_\infty}{T_{0_\infty} - T_\infty}\right)\right]c_{f_\infty}\left(\frac{\rho_\infty a_\infty^3}{2}\right)M_\infty^3 - \frac{\varepsilon\sigma T_w^4}{G} \qquad \textbf{2.19}$$

2.4 Turbulent Flow

The difference between laminar and turbulent flows is the relative steadiness of the two types of flows. In laminar flow, the fluid properties and velocity at each point are actually constant with respect to time, and the fluid flows in "lamina" or in sheets. In a turbulent flow, which is steady in the mean, the local acceleration $\partial u/\partial t$ may be much larger than the convective acceleration $u\,\partial u/\partial x$. In turbulent flow, an additional interaction is due to the transfer of momentum from layer to layer, owing to the velocity

fluctuations. The momentum transport in unit time and through unit area due to the fluctuations represents an apparent shearing stress for the mean motion. This additional apparent shear stress results in skin-friction and heat-transfer coefficients for a turbulent boundary layer that are several orders of magnitude larger than the corresponding values for a laminar boundary layer at the same Reynolds number.

For the case of turbulent flow, the governing equation for aerodynamic heat transfer is similar to the one for the laminar flow. By using the Reynolds analogy, the Stanton number in the case of turbulent flow is related to the local skin-friction coefficient by Eq. 2.20.

$$c_{h_\infty} = 0.6 c_{f_\infty} \qquad \textbf{2.20}$$

In the case of a fully turbulent boundary layer, the recovery factor varies almost exactly as the cube root of the Prandtl number.

$$R_{turb} = \sqrt[3]{\mathrm{Pr}} \qquad \textbf{2.21}$$

Substituting Eqs. 2.20 and 2.21 into 2.5 yields:

$$\frac{q_a}{G} = \frac{0.6}{JG}\left[\mathrm{Pr}^{1/3}\left(\frac{T_{aw} - T_\infty}{T_{aw} - T_\infty}\right)\right] c_{f_\infty}\left(\frac{\rho_\infty a_\infty^3}{2}\right) M_\infty^3 . \qquad \textbf{2.22}$$

The skin-temperature equation for the turbulent flow, using Eqs. 2.5, 2.6 and 2.22 is:

$$\frac{dT_w}{dt} = \frac{1}{JG}\left[0.6\left(\frac{T_{aw} - T_\infty}{T_{0_\infty} - T_\infty}\right)\right] c_{f_\infty} \left(\frac{\rho_\infty a_\infty^3}{2}\right) M_\infty^3 - \frac{\varepsilon\sigma T_w^4}{G}. \qquad \textbf{2.23}$$

2.5 Conclusion

Equations 2.19 and 2.23 are used to calculate the skin temperature for laminar and turbulent flow in the case of a flat plate. In the case of laminar flow, the same equation can also be used for cones. But for turbulent flow, the Reynolds number must be divided by 2 in order to incorporate the cone rule. (For the same cone Mach number and wall-to-free-stream temperature, the cone solution for the local skin friction is the same as the flat-plate solution when the cone Reynolds number is divided by 2.)

3 Determination of Parameters

The formula for the calculation of the wall temperature involves a lot of parameters which vary with the altitude and wall temperature. All these parameters need to be calculated before integration of the governing equations can be carried out.

3.1 Atmospheric Data

In general, the time history of the flight path (velocity in ft/sec and the altitude in feet versus time in seconds) is known in advance. Based on this information the time history of the ambient (true free-stream) temperature, static pressure and density of the air can be determined from the standard atmospheric tables. This standard atmosphere is mathematically defined in six layers from sea level to 71 km, as shown in Table 3.1 S.

Table 3.1 Standard atmospheric layers [28].

Layers	Name	Lower Altitude (km)	Upper Altitude (km)	Upper Altitude (ft)
1	Troposphere	0	11	36,089
2	Stratosphere	11	20	65,618
3	Stratosphere	20	32	104,987
4	Stratosphere	32	47	154,199
5	Stratosphere	47	51	167,323
6	Mesosphere	51	71	232,940

Using the relations given in Table A.1 (Appendix 1), we can obtain a reasonably accurate model of the standard atmosphere up to 71 km that is consistent with the results displayed in Figure 3.1. Values of the ambient (true free-stream) temperature, static pressure and density of the air above 71 km can be determined from the U.S standard atmospheric tables, 1976. Using the values of static temperature, the ambient speed of sound is calculated by:

$$a_0 = 49.028 \times T_0^{(1/2)}. \qquad \textbf{3.1}$$

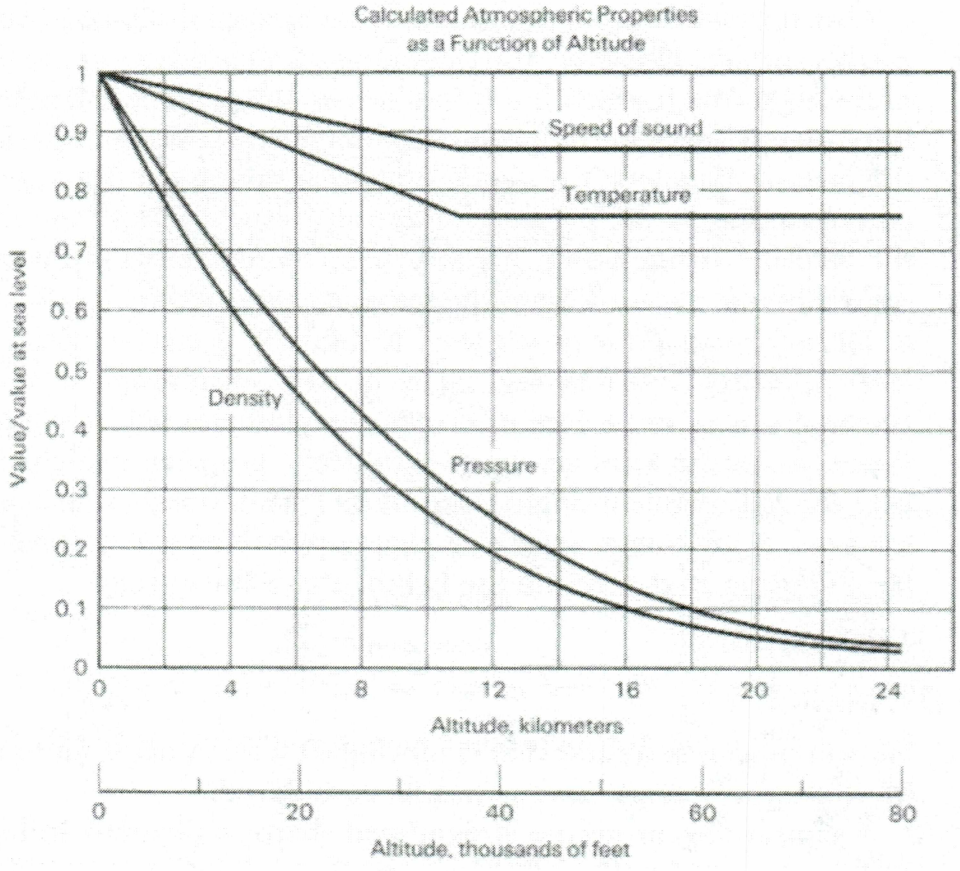

Figure 3.1 Standard atmospheric properties as a function of altitude [29].

Likewise, from the time history of the velocity in ft/sec and the speed of sound in ft/sec, the value of the free-stream Mach number with respective to time can be calculated.

3.2 Local Free Stream Values

Using the time history of the free-stream Mach number and the cone angle, the time history of the local Mach number M_∞, local temperature T_∞, local density ρ_∞ and

the local speed of sound a_∞ can be calculated using the supersonic tables [27]. Figure 3.2 shows the location of the local free-stream values with respect to the free-stream values.

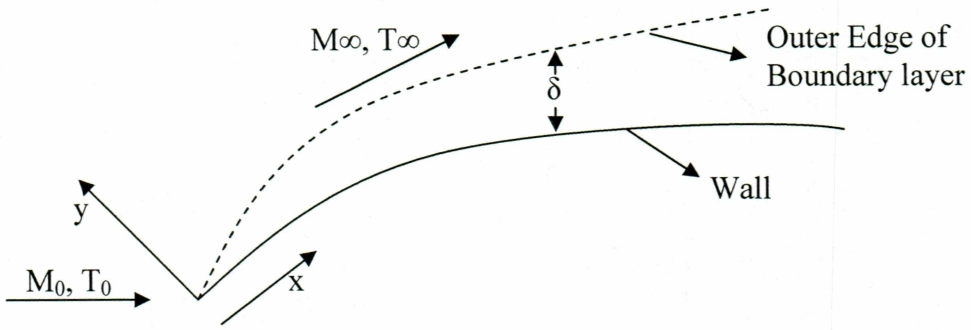

Figure 3.2 Boundary layer notation [1].

The solution used in these supersonic tables is calculated by the method of characteristics and requires that the flow conditions along a starting line in the flow field be known. The results are given in an x, r cylindrical coordinate system that has its origin at the cone vertex. The differential equation that is the formulation of the conical flow problem in a spherical coordinate system is:

$$\frac{d^2u}{d\theta^2}+u=\frac{a^2(u+v\cot\theta)}{v^2-a^2} \qquad \textbf{3.2}$$

$$v=\frac{du}{d\theta} \qquad \textbf{3.3}$$

$$a^2=\frac{\gamma-1}{2}(1-u^2-v^2). \qquad \textbf{3.4}$$

In the forgoing equations, all the velocities are non-dimensionalized by dividing them by the limiting velocity attainable by adiabatic expansion into a vacuum. This system of computation was used, even though the results are later transposed into another

reference system, in order to make use of the parameters as convenient guides in setting up the numerical calculations. Boundary conditions must be prescribed along with Eq. 3.2 to 3.4, and they are given by Eq. 3.5 at the surface of the cone.

$$\left.\begin{aligned} u &= u_s \\ v &= 0 \end{aligned}\right\} \qquad \textbf{3.5}$$

The upper boundary condition is found by requiring the results obtained by the integration of Eq. 3.2 to satisfy the Rankine-Hugoniot equations which can be expressed as:

$$\tan\theta = \left(\frac{\gamma-1}{\gamma+1}\right)\left(\frac{u^2-1}{uv}\right). \qquad \textbf{3.6}$$

When Eq. 3.6 is fulfilled by the results from Eq. 3.2, the local free-stream Mach number is given by:

$$M_\infty = \sqrt{\left(\frac{2}{\gamma-1}\right)\left(\frac{u^2}{\cos^2\theta - u^2}\right)}. \qquad \textbf{3.7}$$

The solutions of Eq. 3.2 presented herein were obtained using the Runge-Kutta integration method. Computations started at the solid surface of the cone by specifying a value of u_s and ended when the shock-wave conditions were satisfied. Integration of Eq. 3.2 yields values of u, v and a at each conical ray angle θ. The results are tabulated for each cone angle as a function of nominal free-stream Mach number in Table A. 2, Table A.3 and Table A.4. (Appendix 1) [27].

Based on the value of the local free-stream temperature, the local free-stream speed of sound is calculated as:

$$a_\infty = \sqrt{\gamma R T_\infty}\,. \qquad \textbf{3.8}$$

In order to pick off the values of the local skin-friction coefficient at each second of the trajectory, it is necessary to calculate the local free-stream Reynolds number. It is calculated as:

$$\mathrm{Re}\, y_\infty = \frac{\rho_\infty V_\infty l}{\mu_\infty} \qquad \textbf{3.9}$$

where $V_\infty = M_\infty \times a_\infty$.

And the local free-stream coefficient of viscosity (using Sutherland's law) is given by Eq. 3.10.

$$\mu_\infty = 3.73\times 10^{-7}\left(\frac{T_\infty}{519}\right)^{1/2}\left[\frac{1+.505(T_\infty/519)}{1.505}\right] \qquad \textbf{3.10}$$

3.3 Stagnation Temperature Rise

In order to take into account the fact that c_p varies with the temperature, it is necessary to integrate the simple energy equation:

$$\int_{V_\infty}^{0} V dV + \int_{T_\infty}^{T_{0_\infty}} J g c_p dT = 0\,. \qquad \textbf{3.11}$$

For constant values of c_p, the above equation becomes:

$$T_{0_\infty} - T_\infty = \frac{1}{2}\frac{V_\infty^2}{Jgc_p}, \qquad \textbf{3.12}$$

where J = mechanical equivalent of heat (778 ft-lb/Btu).

For the actual case, c_p varies with temperature. It has been found that a correction for variable c_p lowers the stagnation temperature considerably at high velocity (for example, 20 percent lower at M_∞ = 8). An exact solution of the above equation for variable c_p gives a set of stagnation temperature curves for various altitudes and Mach numbers. We also know that plotting the stagnation temperature rise $T_{0_\infty} - T_\infty$ versus free-stream velocity V_∞ gives a single curve for all altitudes. For all practical purposes, the plot between $T_{0_\infty} - T_\infty$ and V_∞ with T_∞ taken as a parameter falls onto a single curve for all values of T_∞ ranging from 392^0 R to 630^0 R, corresponding to the minimum and maximum free-stream temperature from sea level to about 370,000 ft. The values of local free-steam velocity and stagnation temperature rise are tabulated in Table A.8 (Appendix 1).

3.4 Skin Friction Coefficient

Of all the parameters discussed so far, calculation of the instantaneous skin friction coefficient is one of the most important parameters. It is possible in this problem, as well as in other similar trajectories, that most of the flight will involve predominantly turbulent flow. But if the altitude and the speed at the end of the trajectory are such that the Reynolds number is less than the transition Reynolds number, the flow can become laminar. So, the skin friction coefficient is calculated using two different formulas based on the nature of the flow.

3.4.1 Laminar Skin Friction Coefficient

As already stated above, the transition of flow from laminar to turbulent is based on the local Reynolds number. In the laminar flow regime, the flow can also experience laminar slip flow during some parts of the flight. The laminar skin friction coefficient equation used below assures that either laminar continuum or laminar slip flow, whichever exists, will be taken care of automatically. The laminar skin friction coefficient for a flat plate is given by:

$$c_{f_\infty} = \frac{1}{M_\infty}\sqrt{\frac{T_\infty}{T_w}} M^* {c_f}^* \qquad \textbf{3.13}$$

where

$$M^* c_f^* = \sqrt{\frac{8}{\gamma\pi}}\, erfc\left(\frac{1.356\sqrt{\mathrm{Re}\, y^*}}{\sqrt{\gamma} M^*}\right) \exp\left(\frac{1.356\sqrt{\mathrm{Re}\, y^*}}{\sqrt{\gamma} M^*}\right) \qquad \textbf{3.14}$$

$$\mathrm{Re}\, y^* = \mathrm{Re}\, y_\infty \left(\frac{T_\infty}{T_w}\right)^{1.76} \qquad \textbf{3.15}$$

$$M^* = M_\infty \left(\frac{T_\infty}{T_w}\right)^{0.5}. \qquad \textbf{3.16}$$

Where the superscript * indicates that the parameters are based on the state properties evaluated at the wall. In order to get the skin friction coefficient for a cone like body, the skin friction coefficient for the flat plate is to be multiplied with $\sqrt{3}$ (Cone rule).

3.4.2 Turbulent Skin Friction Coefficient

The turbulent skin friction coefficient for a flat plate with arbitrary wall temperature, free-stream Reynolds number and Mach number is given by Eq. 3.17 and the nomograph for the coefficient of friction on a flat plate is given in Figure 3.3. Even though some parts of the flight are expected to be in the turbulent slip flow regime, this is not considered, since no knowledge exists of skin friction coefficients under turbulent flow outside the continuum regime. Then in order to get the skin friction coefficient for a cone-like body, half of the normal Reynolds number is used (cone rule for turbulent flow, [1]).

$$\frac{0.242}{A\left(c_{f_\infty}\right)^{1/2}\left(T_w/T_\infty\right)^{1/2}}\left(\sin^{-1}\alpha+\sin^{-1}\beta\right)=0.41+\log_{10}\mathrm{Re}\,y_\infty c_{f_\infty}-\frac{1+2n}{2}\log_{10}\left(\frac{T_w}{T_\infty}\right) \quad \textbf{3.17}$$

Where

$$\alpha=\frac{2A^2-B}{\left(B^2+4A^2\right)^{1/2}};\beta=\frac{B}{\left(B^2+4A^2\right)^{1/2}} \quad \textbf{3.18}$$

$$A^2=\frac{[(\gamma-1)/2]M_\infty^2}{T_w/T_\infty};B=\frac{1+[(\gamma-1)/2]M_\infty^2}{T_w/T_\infty}-1 \quad \textbf{3.19}$$

3.5 Material Properties

The skin material to be used may or may not be fully decided upon. For a given body and material, the specific weight w in lb/ ft^3 and the thickness t_s in feet are constants. The specific heat of the skin material, c, in Btu/lb-°R, is a function of the skin temperature. Thus, the heat-absorption capacity of the skin material, G, in Btu/ ft^2-°R, can be expressed as:

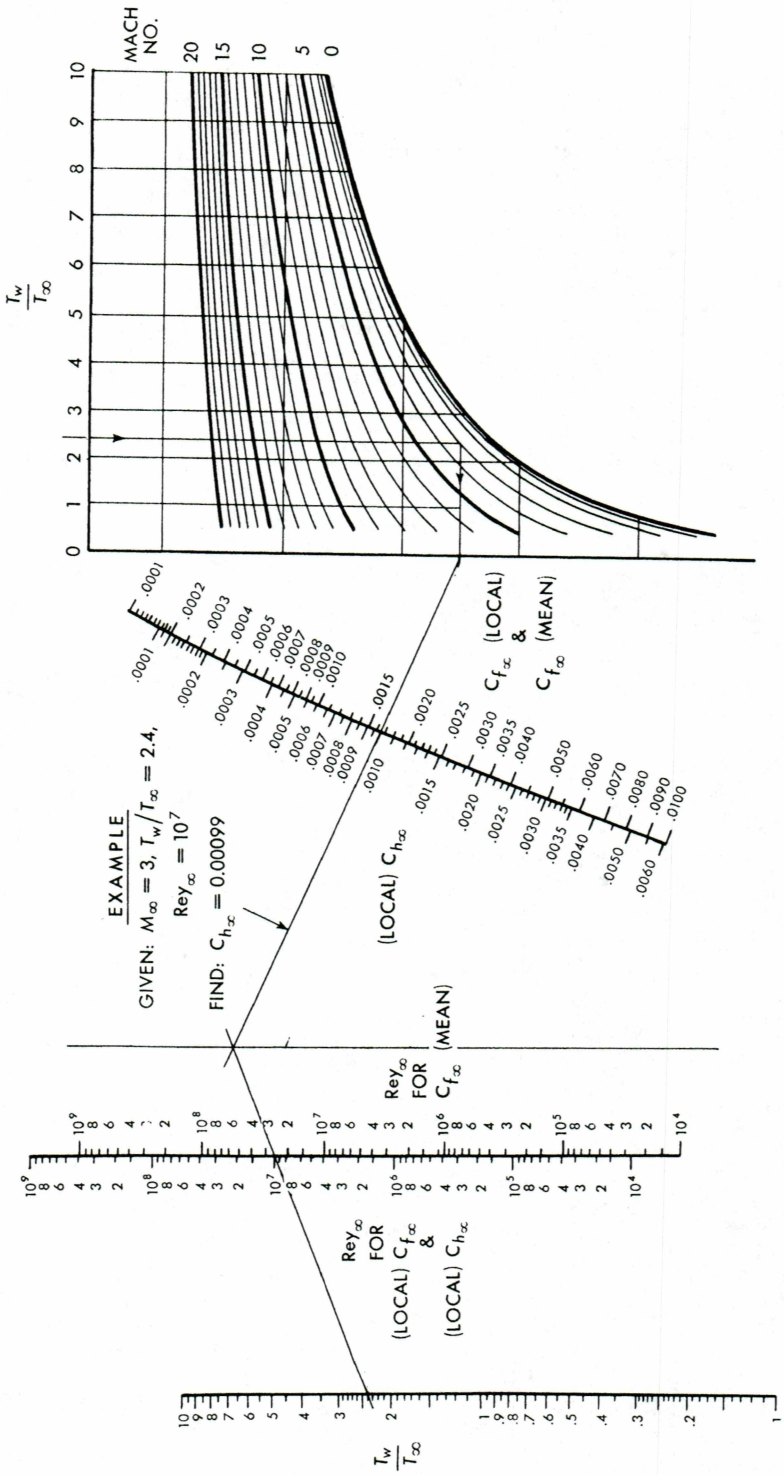

Figure 3.3 Nomograph for coefficient of friction of a turbulent boundary layer on a flat plate [1].

$$G = ct_s w. \qquad \textbf{3.20}$$

This is a function of the temperature. In order to calculate the instantaneous value of G, it is necessary to have the tabulated values of specific heat of the skin material for a wide range of temperatures. Table A.9 (Appendix 1) contains the specific heat of the skin material used in the current simulations from 460^0 R to 2600^0 R.

3.6 Conclusion

Once all the parameters are calculated, Eq. 3.21, which is a nonlinear equation with variable coefficients of first order but the fourth degree, is solved using the Runge-Kutta numerical integration method.

$$\frac{dT_w}{dt} = f(T_w, t) \qquad \textbf{3.21}$$

To explain further, the solution of the differential equation 3.21, which reduces to $T_w = T_0$ when $t = t_0$, is obtained, with the tabular interval being Δt. Then the fourth order Runge-Kutta method of numerical integration is carried out in the following self-explanatory scheme:

Table 3.2 The Runge-Kutta numerical integration method [1]

t	T_w	f	$f * \Delta t$	Operation
t_0	T_0	f	q_1	$\frac{1}{2}(q_1+q_4)$
$t_0+\Delta t/2$	$T_0+q_1/2$	f	q_2	q_2+q_3
$t_0+\Delta t/2$	$T_0+q_2/2$	f	q_3	Sum
$t_0+\Delta t$	T_0+q_3	f	q_4	q=1/3 sum
$t' = t_0+\Delta t$	$T'=T_0+q$	f		

The process is repeated using (t', T') as the pair of initial values, so the skin temperature corresponding to $t = t_0+2\Delta t$ can be computed.

4 Simulink Model

4.1 Introduction

SIMULINK® is a software package that enables us to model, simulate, and analyze systems which are time dependent. Such systems are often referred to as dynamic systems. It supports linear and nonlinear systems, modeled in continuous time, sampled time, or a hybrid of the two. SIMULINK® can be used to explore the behavior of a wide range of real-world dynamic systems, including mechanical systems, electrical systems, thermodynamic systems, biological systems, etc.

Simulating a dynamic system in SIMULINK® is a two-step process. The first step consists of creating a graphical model of the system to be simulated using mathematical blocks of the SIMULINK® model editor. The model depicts the time-dependent mathematical relationships among the system's inputs, states, and outputs. The second step includes simulating the behavior of the system over the specified time span. The information entered into the model is used by SIMULINK® to perform the simulation.

4.2 Defining a Model in SIMULINK®

There are two phases in order to utilize SIMULINK®, the model definition phase and model analysis phase. A typical session starts with either creating a new system model in terms of block diagrams from a library of standard components or recalling a previously defined model, then proceeding to analyze the model. Models are created and manipulated in the block diagram windows primarily by mouse driven commands. One can build an entire SIMULINK® model by the use of extensive block libraries provided in the software. Most of the commonly used linear and nonlinear control system entities are available as predefined blocks in SIMULINK®. Alternatively, new blocks or libraries of tools for analysis can be built and defined. Once the model is completely developed in the interface window, it can be analyzed by choosing options either from the simulation

menu or by executing MATLAB™ commands from the command line in the main MATLAB™ window.

4.3 Simulink Model

The aerodynamic heating problem has been modeled in SIMULINK® and the top level block diagram is shown in Figure 4.1. This model consists mainly of six blocks that were connected together. The first block is the input block whereas the second, third, fourth and the fifth blocks are used to calculate 1st, 2nd, 3rd and 4th coefficients of the Runge-kutta numerical method along with the different parameters required for the simulation. Each of these blocks consists of seven subsystems. SIMULINK® has the flexibility to include subsystems. As the model increases in size and complexity, the structure can be simplified by grouping blocks into subsystems. This helps in reducing the number of blocks displayed in the model window and also allows us to keep the functionally related blocks together.

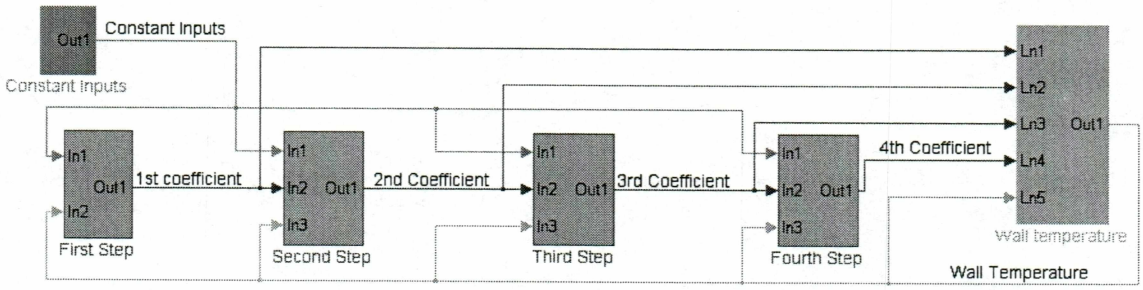

Figure 4.1 SIMULINK® model.

Figure 4.1 shows the structure of the overall SIMULINK® model. Based on the parameters from all the preceding blocks, the *Wall Temperature* block is used to calculate the wall temperature using the Runge-Kutta numerical method. After entering all the input vales in the respective blocks, the simulation is run by clicking the start button in SIMULINK®.

4.4 Constant Inputs Block

Figure 4.2 shown below is the *Constant Inputs* block. The block provides all the inputs to the simulation that are constant throughout the span of the simulation. The block consists of eight inputs that are merged into a single output using the *Mux* block. The single output from this block carries all the eight input values as one signal.

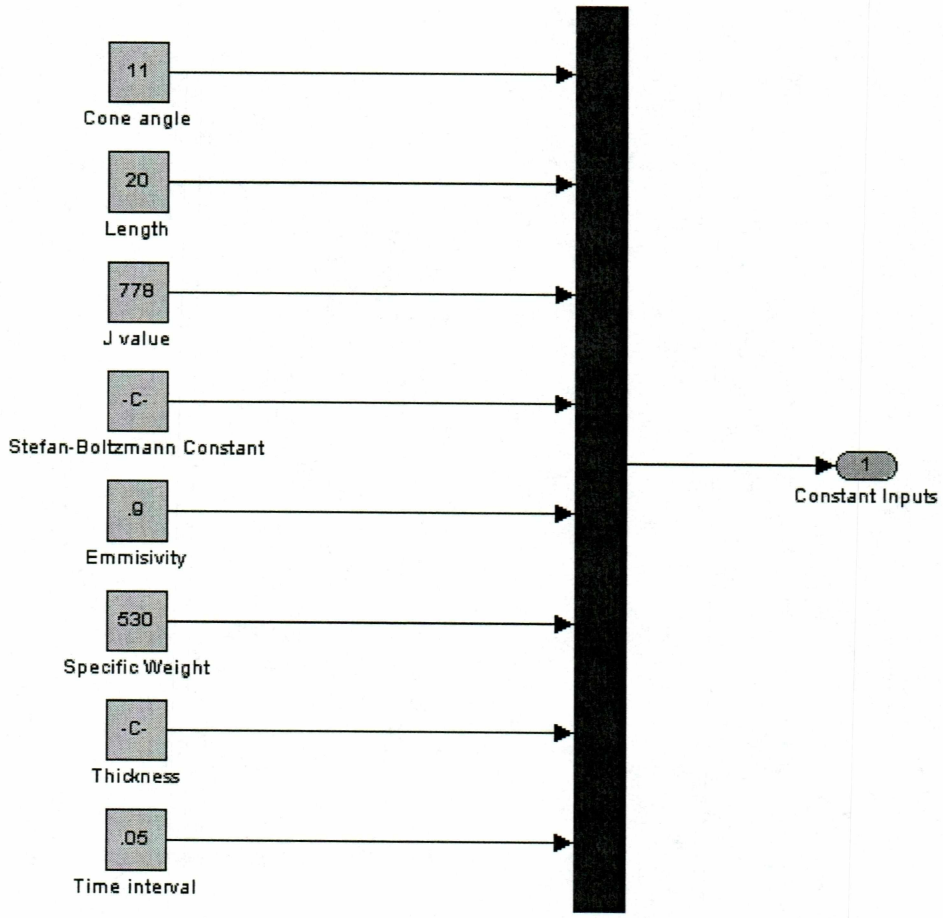

Figure 4.2 SIMULINK® model of the *Constant Inputs*.

4.5 Step-One Model

Figure 4.3 shown below is the *Step-One* block which is explored in detail in the following sections. This model has 2 inputs and 1 output. The inputs are the constant values from the *Constant Values* block and the wall temperature from the previous time step. The output is the 1st coefficient of the Runge-kutta method multiplied by the time interval.

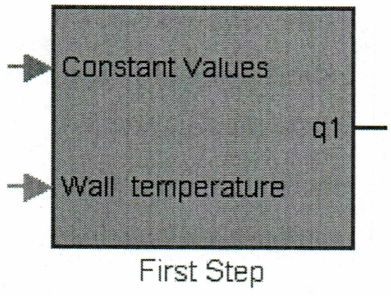

Figure 4.3 SIMULINK® model of the *Step One block.*

The model consists of seven different subsystems contained in blocks. The description of each block is outlined in the subsequent sections.

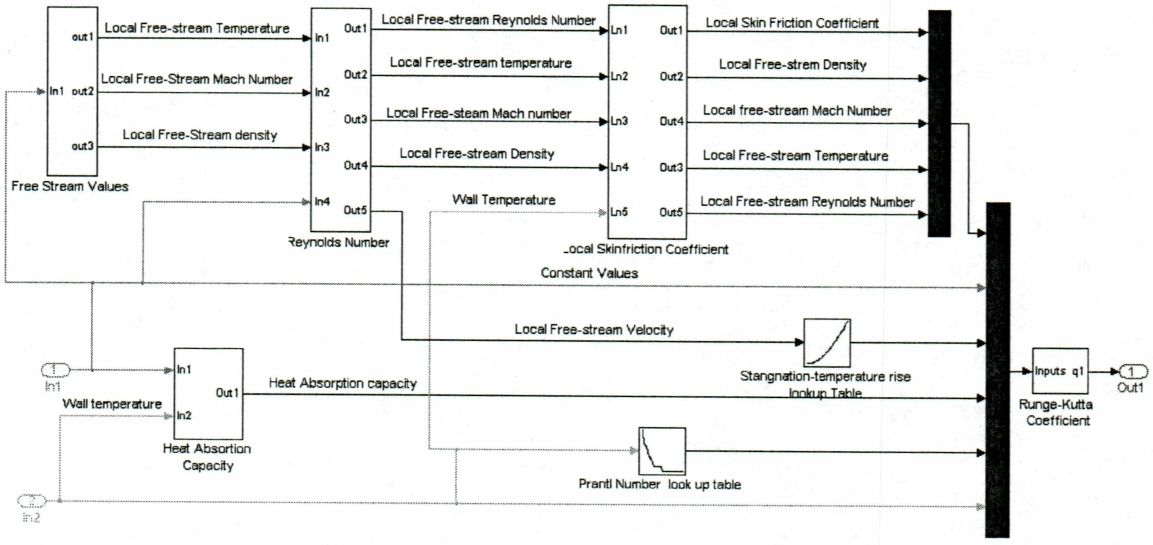

Figure 4.4 SIMULINK® model of the *Step One.*

4.5.1 Free Stream Values

The details of the subsystem *Free Stream Values* block are shown in Figure 4.5. This block consists of two subsystems including the *Atmospheric Data* block and the *Local Free Stream Values* block. The *Atmospheric Data* block is shown in Figure 4.6.

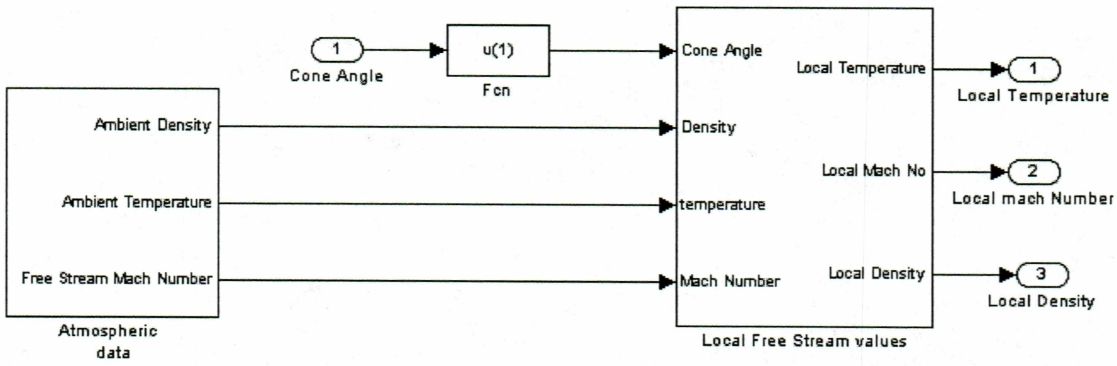

Figure 4.5 SIMULINK® model of the *Free Stream Values* block.

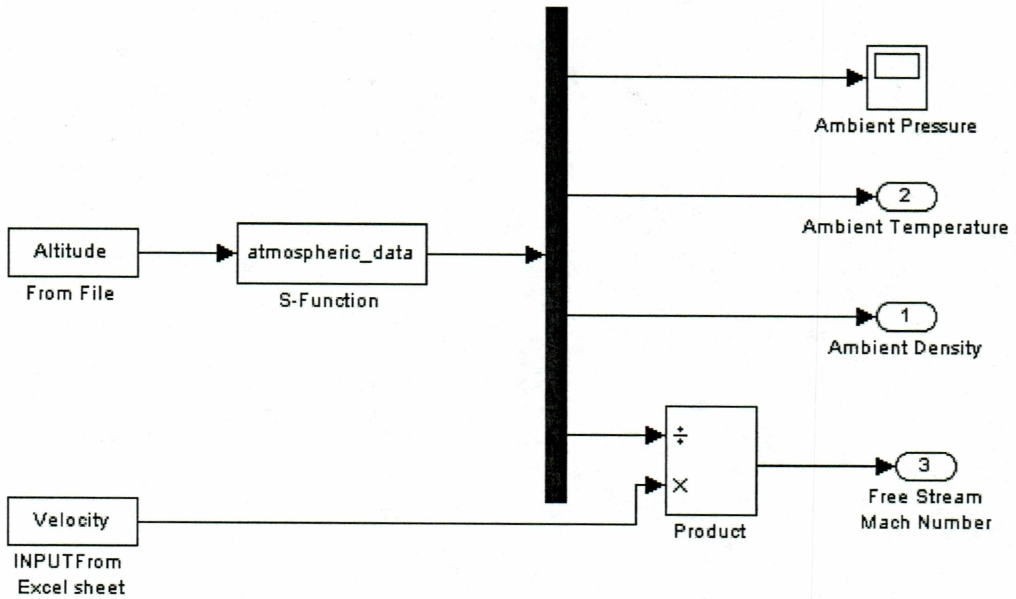

Figure 4.6 SIMULINK® model of the *Atmospheric Data.*

The *Free Stream Values* block includes two input files, which are obtained using the 'from file' functions in SIMULINK®. Altitude and Velocity are .mat files consisting of a matrix with two rows. The first row of the matrix is the time element and the second row of the matrix is the value for the altitude and the velocity, respectively. The other blocks in the system use these values to perform the required operations. The *Atmospheric Data* block is an s-function block that calculates the time history of the ambient temperature, density, pressure and speed of sound. The formulas used in the s-function are given in Table A.1 (Appendix 1). The *Product* block is used to divide the velocity by the speed of sound to obtain the free-stream Mach number.

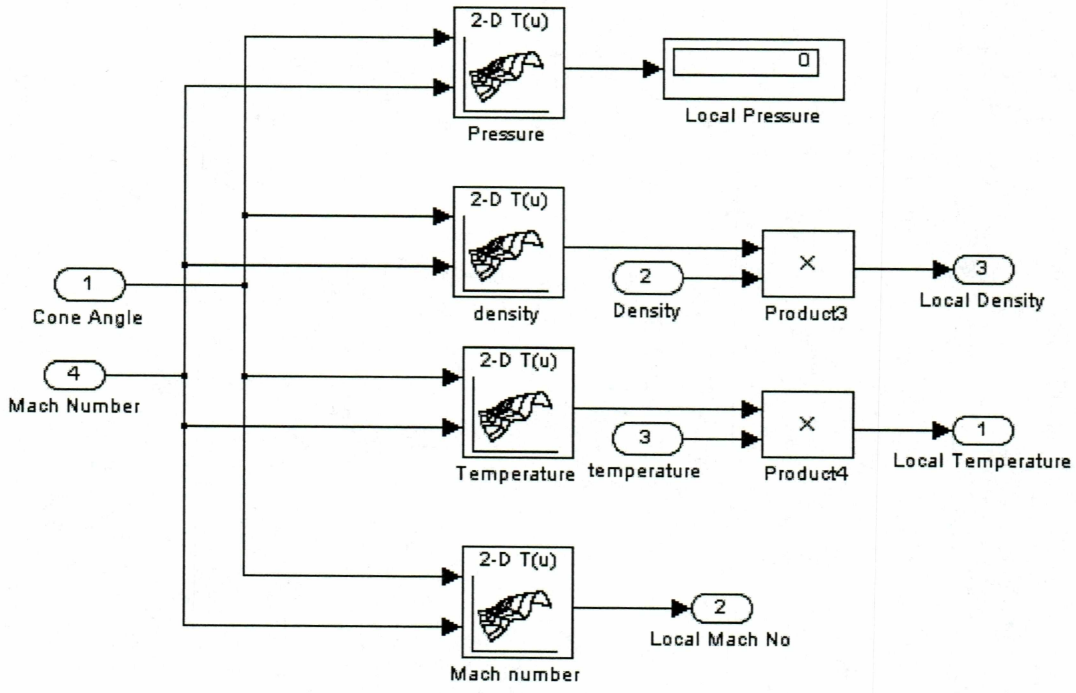

Figure 4.7 SIMULINK® model of the *Local Free Stream Values.*

The *Local Free Stream Values* block is shown in Figure 4.7. The inputs are the cone angle, ambient density, ambient temperature and the free-stream Mach number. The

first three *Look-up* tables were used to calculate the ratio of local free-stream values to free-stream values (pressure, density and temperature) based on the cone angle and the free-stream Mach number, whereas the fourth *Look-up* table is used to calculate the local Mach number based on the cone angle and the free-stream Mach number. The *Look-Up Table* block evaluates a sampled representation of a function in N variables by interpolating between samples to give an approximate value for $y = f(x_1, x_2 \ldots x_n)$, even when the function F is known only empirically. The block generates an output value by comparing the block inputs with the breakpoint set parameters. The look-up table expands to the window shown in Figure 4.8 when selected. The cone angle data, Mach number data and the ratio of the quantities were entered in the first row, second row and table data, respectively. The input data for these tables are given in Table A. 2, Table A.3 and Table A.4. The outputs from the tables two and three were then multiplied with the free-stream values of temperature and density, using the product block to give the local free-stream temperature and density.

In conclusion, the *Free Stream Values* block outputs the local free-stream values of temperature, density and the Mach number.

4.5.2 Local Reynolds Number

The details of the subsystem *Local Reynolds Number* block are shown in Figure 4.9. The purpose of this block is to calculate the free-stream Reynolds number based on Eq. 3.9. The inputs to this block are local free-stream temperature, local free-stream Mach number, local free-stream density and the constant values. The local free-stream coefficient of viscosity is calculated using the *Function* block in SIMULINK® and is based on Eq. 3.10. The local free-stream speed of sound is obtained by multiplying the square root of the local free-stream temperature with the constant value of 49.02 (obtained by substituting the values of the specific heat of air 1716 ft-lb/slug/°R and

specific heat ratio, 1.402, in Eq. 3.8). It is then multiplied with the local free-stream Mach number to get the local free-stream velocity.

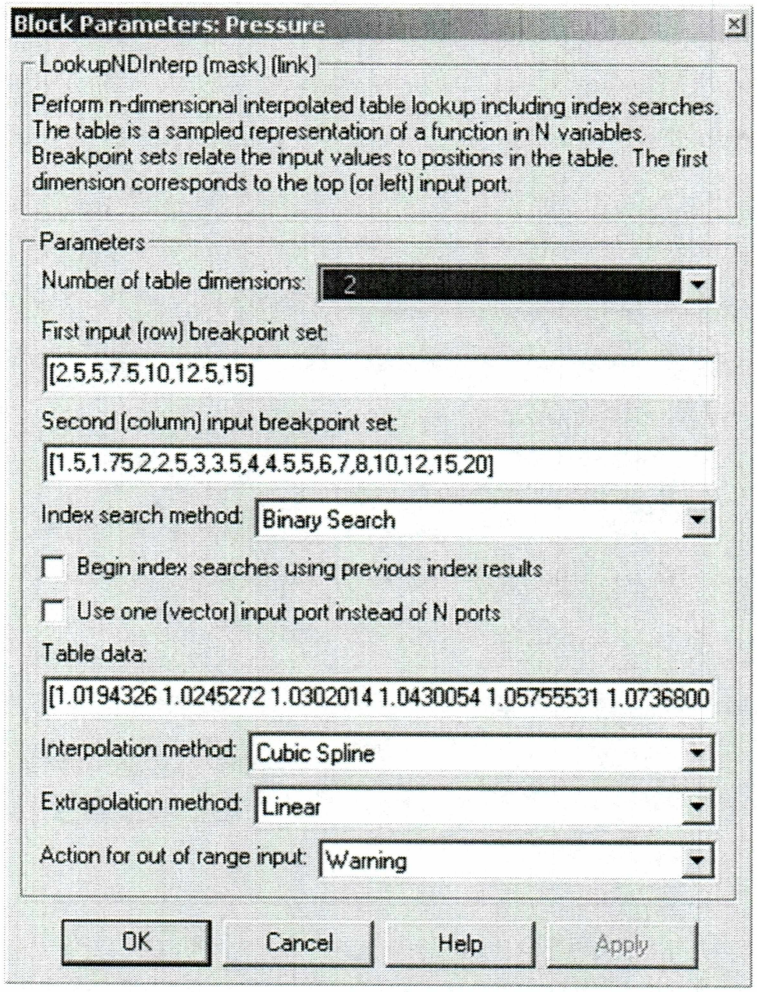

Figure 4.8 Window for the *look-up* table.

Using the *Function* block, the values of local free-stream density, local free-stream velocity and length are multiplied together and divided by the value of local free-stream coefficient of viscosity to get the local free-stream Reynolds number. Along with the free-stream Reynolds number as output, some of the inputs to this block are sent out as outputs to the next block.

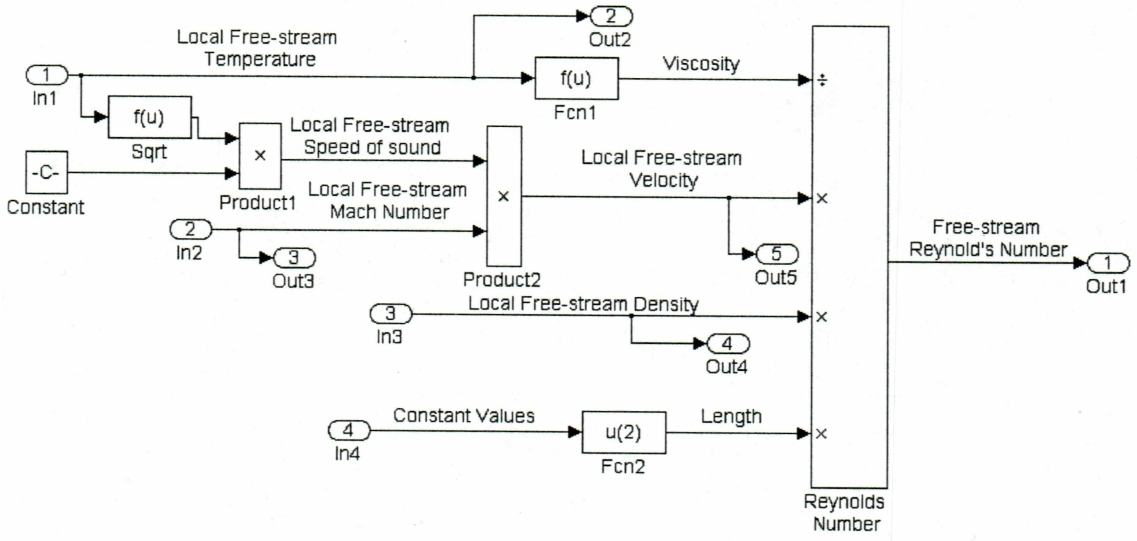

Figure 4.9 SIMULINK® model of the *Local Reynolds Number.*

4.5.3 Local Skin Friction Coefficient

The details of the subsystem *Local Skin Friction Coefficient* block are shown in Figure 4.10. This block calculates the instantaneous values of the skin friction coefficient. The inputs *Ln1*, *Ln2*, *Ln3*, *Ln4* to this block are the four outputs of the *Reynolds Number* block. The input *Ln5* of this subsystem is the wall temperature from the previous time step and the constant block is used to input the specific heat of air. The laminar and the turbulent skin friction coefficients are calculated by using two *Enable Subsystem* blocks. Only one of the two blocks will be executed based on the output obtained from the *Transition* subsystem block, which is used to calculate the transition from the laminar to turbulent flow. The output from the laminar and the turbulent subsystems are added together using a *Sum* block to get the local skin friction coefficient. Along with the local skin-friction coefficient as output, some of the inputs to this block are sent out as outputs to the next block.

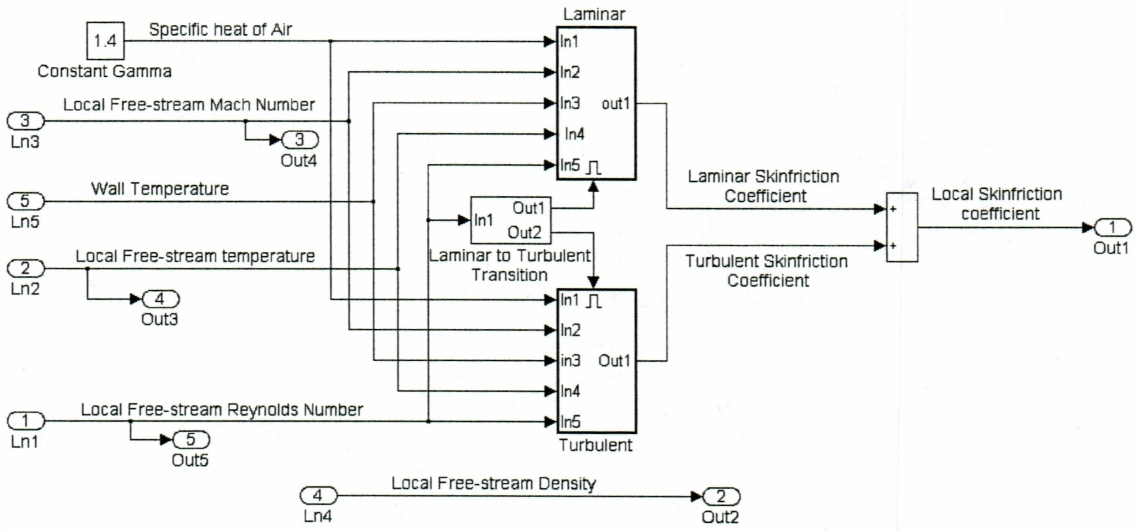

Figure 4.10 SIMULINK® model of the *Local Skin Friction Coefficient.*

4.5.3.1 Laminar to Turbulent Transition

The details of the subsystem *Laminar to Turbulent Transition* block are shown in Figure 4.11. This block enables the laminar and the turbulent skin friction block based on the transition Reynolds number. The input *Ln1* to this block is the local free-stream Reynolds number. The other input to the block is the transition Reynolds number. This block is masked so the block expands to the window shown in Figure 4.12 when selected. The user is required to enter the values of the transition Reynolds number used in the model.

Two relational operators (performs a relational operation on its two inputs and produces output 1 if TRUE and 0 if FALSE), *Relational Operator1* and *Relational Operator2*, are used to compare the local free-stream Reynolds number with the transition Reynolds number and output zero or one based on the comparison. This result in the execution of one of the two enable blocks (*Laminar* or *Turbulent Skin Friction* blocks).

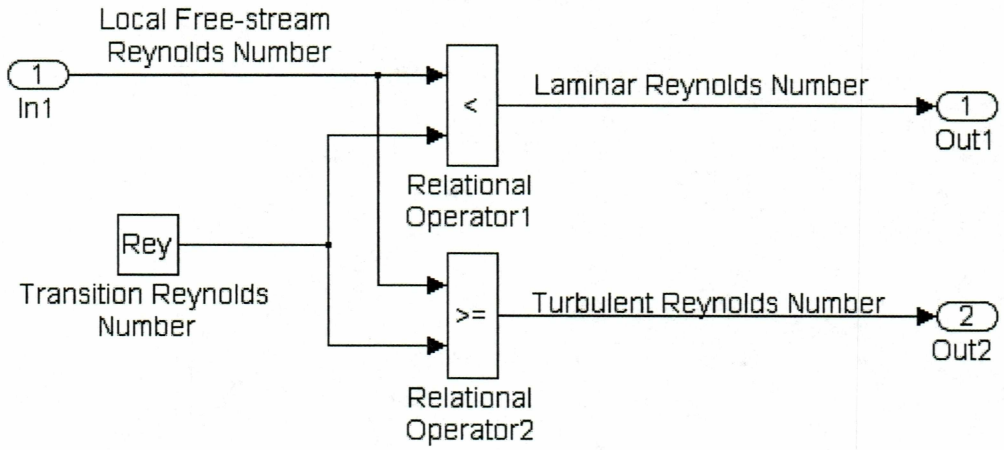

Figure 4.11 SIMULINK® model of the *Laminar to Turbulent Transition.*

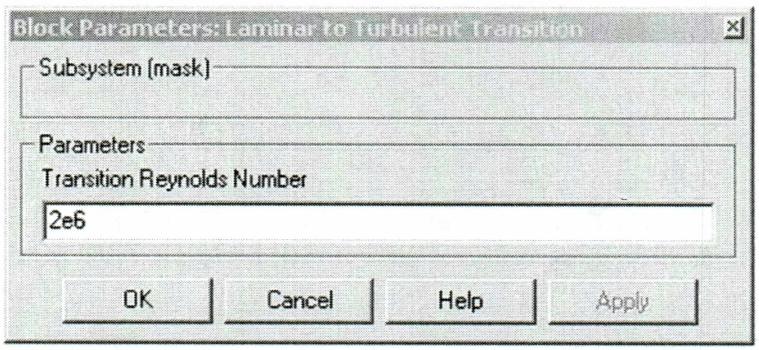

Figure 4.12 Window for the *Transition Reynolds Number.*

4.5.3.2 Local Laminar Skin Friction Coefficient

The details of the subsystem *Local Laminar Skin Friction Coefficient* block are shown in Figure 4.13. This block calculates the instantaneous values of the local laminar skin friction coefficient whenever the output *Out1* in the laminar to turbulent transition is one. The inputs *Ln1*, *Ln2*, *Ln3*, *Ln4* and *Ln5* to this block are the five outputs of the *Local Skin Friction Coefficient* block. The four inputs of *Ln2*, *Ln3*, *Ln4* and *Ln5* are combined together using the *Mux* in Simulink. The function blocks *Fcn1* and *Fcn2* are used to calculate the wall Mach number and wall Reynolds number. The input *Ln1*, wall Mach number and wall Reynolds number are combined together by using one more *Mux* in SIMULINK®.

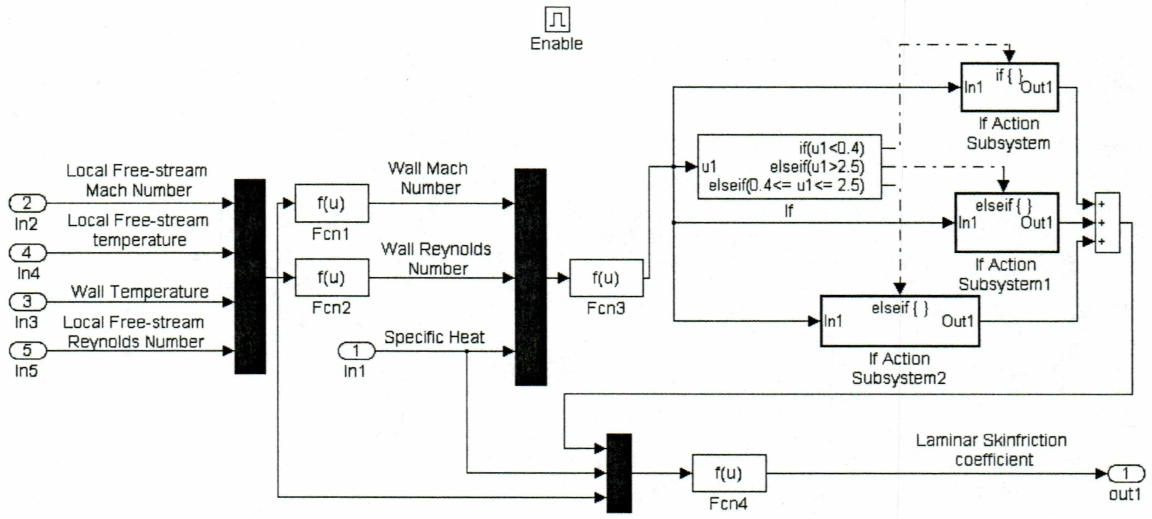

Figure 4.13 SIMULINK® model of the *Laminar Local Skin Fiction Coefficient.*

The parameter $\sqrt{\mathrm{Re}\, y^*}/\sqrt{\gamma}\, M^*$ is calculated by using function block *Fcn3*. The *if* block is used to divide the output based on the value output from the *Fcn3* block and one of the three if action subsystem blocks are used to calculate the value of $\sqrt{\gamma} M^* c_f^*$. The outputs *Out1* of all the three *If Action* blocks are reset to zero whenever the blocks are disabled. Then the outputs from the three action subsystems are added together using a *Sum* block. The output from the *Sum* block, specific heat of air and the output signal from the first *Mux* block, are combined together using another *Mux* block. The function block *Fcn4* is used to calculate the local laminar skin-friction coefficient.

4.5.3.3 Local Turbulent Skin Friction Coefficient

The details of the subsystem *Local Turbulent Skin Friction Coefficient* block are shown in Figure 4.15. This block calculates the instantaneous values of the local turbulent skin friction coefficient whenever the output *Out2* in the laminar to turbulent transition is one. The inputs *Ln1*, *Ln2*, *Ln3*, *Ln4* and *Ln5* to this block are the five outputs of the *Local Skin Friction Coefficient* block. The four inputs of *Ln1*, *Ln2*, *Ln3* and *Ln4* are combined together using the *Mux* in SIMULINK®. The values A^2, B, alpha, and beta

are calculated using *Function* blocks in SIMULINK® and are based on the Eqs. 3.18 and 3.19 respectively. Constants A^2, alpha, beta, input *Ln3* and input *Ln4* are combined together by using one more *Mux* in SIMULINK®. Similarly input *Ln3*, *Ln4*, *Ln5* and constant value n are combined together using another *Mux*. Then functions *Fcn1* and *Fcn2* are used to calculate the values of Eqs. 4.1 and 4.2 respectively.

$$0.242\left(\sin^{-1}\alpha+\sin^{-1}\beta\right)/A\left(T_w/T_\infty\right)^{1/2} \qquad \textbf{4.1}$$

$$0.41+\log_{10}\mathrm{Re}\,y_\infty-\left(1+2n/2\right)\log_{10}\left(T_w/T_\infty\right) \qquad \textbf{4.2}$$

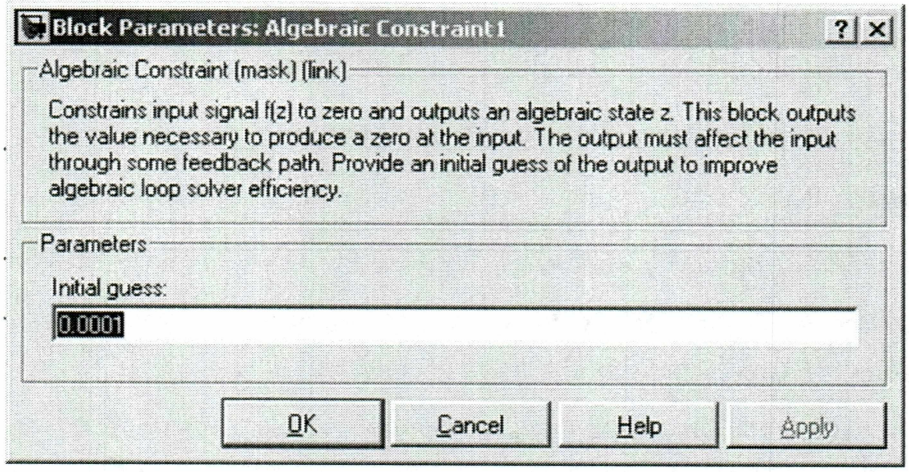

Figure 4.14 Window for entering the initial guess.

The algebraic constraint1 (constrains the input signal f(z) to zero and outputs an algebraic state z) is used to solve Eq. 3.17. The block expands to the window shown in Figure 4.14 when selected and the user needs to enter the initial guess. The feedback loop is used to calculate the values of $c_{f_\infty}^{\,1/2}$ and $\log_{10} c_{f_\infty}$ using the blocks *Fcn3* and *Math Function1* from SIMULINK®, respectively. The output from *Fcn2* is added to *Math Function* and then multiplied with *Fcn3* using a *Product* block from SIMULINK®. At the

end, the signal from the *Fcn2* block is subtracted from the signal from the *Sum* block and the output is sent to the *Algebraic Constraint1* block. Once the algebraic equation is solved to get the value of turbulent skin-friction coefficient, it is multiplied with the output from the *Enable* block (outputs 1 whenever the block is enabled and 0 whenever it is not) to ensure that output resets to zero whenever the block is not disabled.

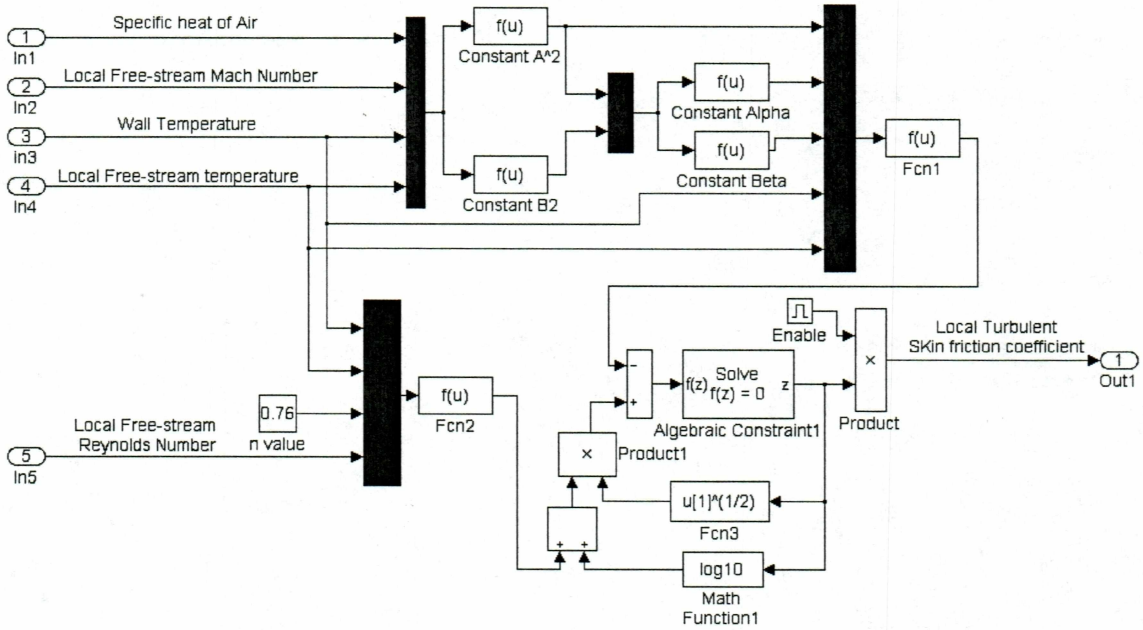

Figure 4.15 SIMULINK® model of the *Turbulent Skin Friction Coefficient.*

4.5.4 Heat Absorption Capacity

The details of the subsystem *Heat Absorption Capacity* block are shown in Figure 4.16. This block calculates the total heat absorption capacity of the skin material, which is a function of the temperature. The two inputs *Ln1* and *Ln2* of this subsystem are the constant values and the wall temperature from the previous time step. The specific weight and the thickness are obtained from *Ln1* using the function blocks *Fcn1* and *Fcn2*. In order to calculate the instantaneous values of heat absorption capacity, it is necessary to have the tabulated values of the specific heat for a wide range of temperatures. The

lookup table consists of the values of specific heat versus temperature. All three values are multiplied together using a *Product* block to get the heat absorption capacity.

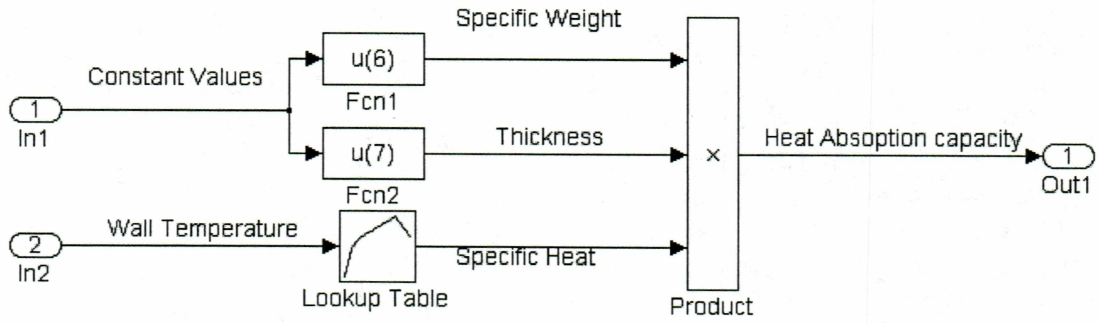

Figure 4.16 SIMULINK® model of the *Heat Absorption Capacity.*

4.5.5 Prandtl Number and Stagnation-Temperature Raise Lookup Tables

An inspection of the equations show that for laminar and turbulent flow solutions, we require tabulated values of the Prandtl number for a wide range of temperatures. The values are as shown in Table A.6 (Appendix 1). The *Prandtl Number* lookup table is used to store these values. The input to this lookup table is wall temperature.

Other important parameters that need to be calculated are the values of $T_{0_\infty} - T_\infty$ versus V_∞. The quantity $T_{0_\infty} - T_\infty$ plotted against V_∞ gives a single curve for all altitudes up to 370,000 ft [1]. The values of $T_{0_\infty} - T_\infty$ and V_∞ are shown tabulated in Table A.8 (Appendix 1). This data is incorporated into the model using a lookup table that gives stagnation temperature rise. The lookup table outputs the value of the temperature difference based on the local free-stream velocity as the input.

4.5.6 Runge-Kutta Coefficient Block

The details of the subsystem *Runge-Kutta Coefficient* block are shown in Figure 4.17. This block calculates different coefficients of the Runge-Kutta numerical method.

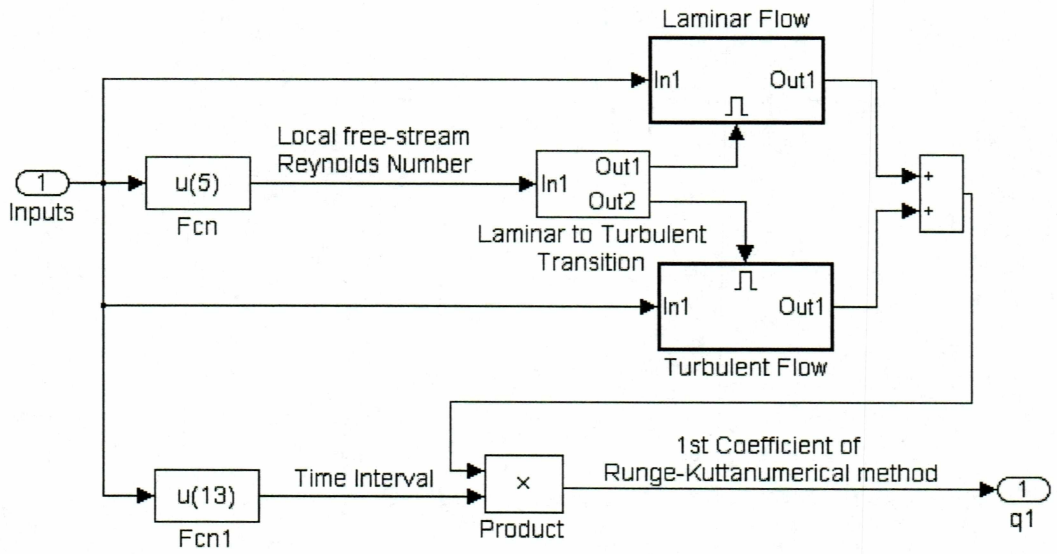

Figure 4.17 SIMULINK® model of the *Runge-Kutta Coefficients.*

The input *Ln1* to this block consists of data of all the parameters from all the preceding blocks. Functions *Fcn* and *Fcn1* are used to separate the *Local Free Stream Reynolds Number* and time interval from all the other inputs. *Laminar Flow*, *Turbulent Flow* and *Laminar to Turbulent Transition* are the three subsystems in this block. The *Laminar Flow* and the *Turbulent Flow* are two enable blocks used to calculate the value of Eqs. 3.45 and 3.46, respectively. These blocks are implemented based on the output from the *Laminar to Turbulent Transition* block. The *Laminar to Turbulent Transition* block is the same as the one used in the *Skin Friction Coefficient* block. The outputs from both of the enable blocks are reset to zero whenever the blocks are disabled. The outputs from the two enable blocks are then added together and multiplied with the time interval to get the 1st coefficient of the Runge-Kutta numerical method.

4.6 Second, Third and Fourth Time Step Block

The details of the subsystem *Second Step* block are shown in Figure 4.18. Each of these three blocks have 3 inputs and 1 output. The inputs *Ln1*, *Ln2* and *Ln3* are constant values from the constant values block, the output from the previous time step block, and the wall temperature from the previous time step. The outputs *q2*, *q3*, and *q4* of these blocks are the 2nd, 3rd, and 4th coefficients of the Runge-Kutta method (Table 3.2) multiplied by the time interval. These blocks are the similar to the *First Step* Block with some small modifications which are discussed in the following sections.

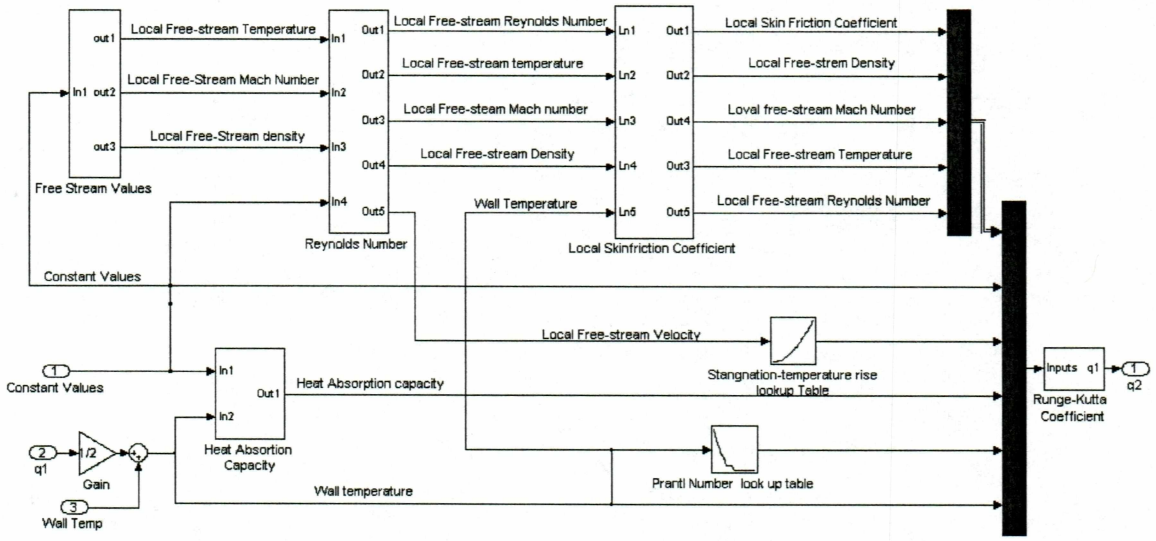

Figure 4.18 SIMULINK® model of the *Second Time-Step.*

In the second time step, one difference is that the input *Ln2* of this block is divided by two using a gain block and then added with the wall temperature from the previous time step to get the wall temperature required for this block. The other difference is that the two mat files *Altitude1.mat* and *Velocity1.mat* are used as input files in place of the *Altitude.mat* and *Velocity.mat* in the *Atmospheric Data* block. The third time step is also the same as the second time step block other than that the *Ln2* of this block is the output from the second time step block. In the fourth time step two mat files

Altitude2.mat and *Velocity2*.mat, are used as the input files Altitude and Velocity in the *Atmospheric Data* block. In the fourth time step, the input *Ln2* of this block is added with the wall temperature from the previous time step to get the wall temperature required for this block.

4.7 Wall Temperature Block

The details of the subsystem *Wall Temperature* block are shown in Figure 4.19. This block calculates the wall temperature by the Runge-Kutta numerical method.

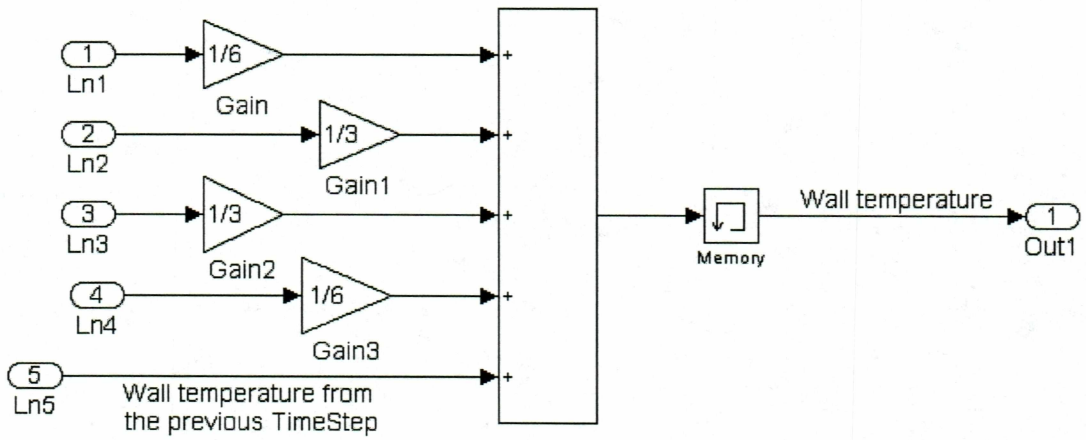

Figure 4.19 SIMULINK® model of the *Wall Temperature* block

The inputs *Ln1*, *Ln2*, *Ln3* and *Ln4* are the 1st, 2nd, 3rd and 4th coefficients of the Runge-Kutta numerical method, respectively, and the input *Ln5* is the wall temperature from the previous time step. The inputs *Ln1*, *Ln2*, *Ln3*, and *Ln4* are multiplied with different gain factors to get the required fraction of the coefficients and then added with the input *Ln5* using a *Sum* block to get the wall temperature of the skin material at the current time. The output from the *Sum* block is then sent to a *Memory* block that is used to input the initial condition for the wall temperature. The *Memory* block expands to the window shown in Figure 4.20 when selected and the user is required to input the initial

condition of the wall temperature. The output from the *Memory* block is then directed to the *Step One* block as input *Ln2*.

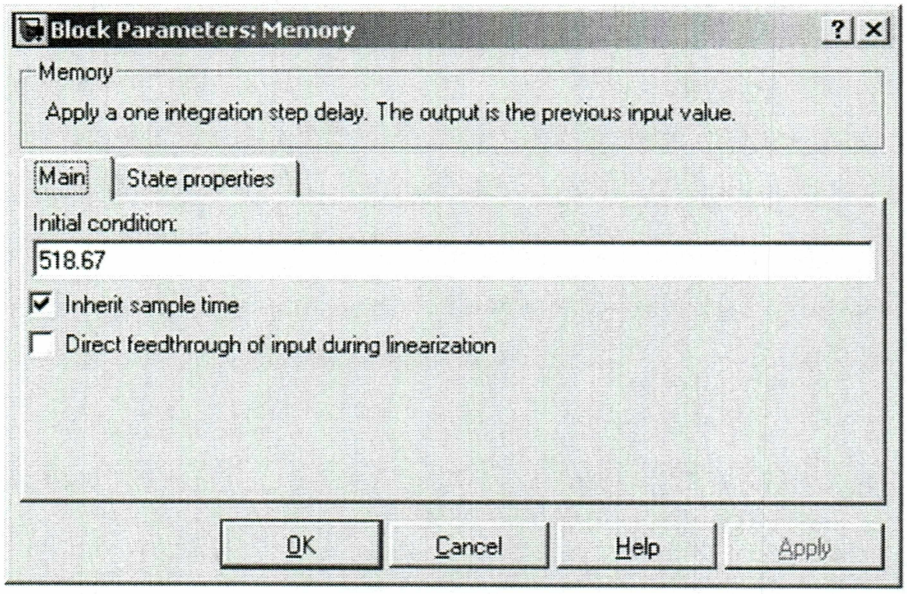

Figure 4.20 Window of the *Memory* block to enter the initial guess for wall temperature.

5 Example Problem

5.1 Introduction

In order to demonstrate the calculation procedure using SIMULINK®, the solution of an example problem is carried out in some detail. The example missile is assumed to be a simple ogival body, 40 ft in length, with the proposed flight trajectory shown in Figure 5.1. The skin material is taken to be non-oxidized Inconel; thickness $t_s = 0.000417$ ft; $w = 530$ lb/ft^3; and emissivity, $\varepsilon = 0.9$. In the present problem, the skin temperature is predicted for a point located 20 ft. back from the nosecone tip. For simplicity it is assumed that this location is on the ogive, and that the local pressure coefficient is zero, so that the local conditions are the same as the free-stream values. In order to incorporate the inputs for the example, a few changes were made in the SIMULINK® model.

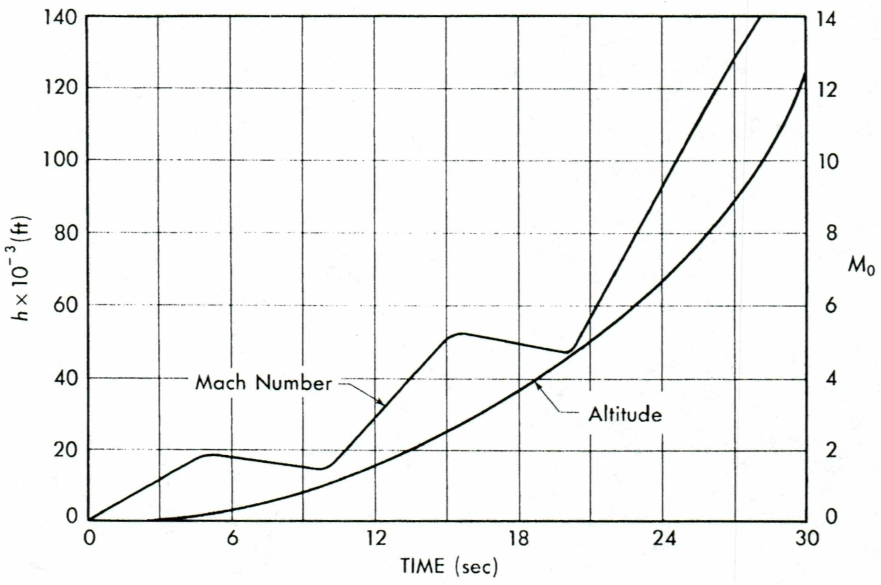

Figure 5.1 Altitude and Mach number versus time for given trajectory [1].

5.2 Inputs for the Example Problem

For a given flight trajectory, certain parameters are either known or must be calculated. In general, the time history of the flight path is known in advance. Based on these data, the free-stream density ρ_0, speed of sound a_0, and the Mach number M_0 for each second of the flight will be measured using a radiosonde at the launching area or calculated using atmospheric tables. For the present problem the values of ρ_0, T_0 and M_0 are directly given. The values of all these parameters are given in Table A.7 (Appendix 1). The next step is to calculate the flow parameters T_∞/T_0, ρ_∞/ρ_0 and M_∞/M_0 for the body station where the skin temperature is to be calculated using the tables for supersonic flow around right circular cones at zero angle of attack [27]. But as discussed above, the body station for the present problem is assumed to have a local pressure coefficient equal to zero. This results in the ratio of the local free-stream values to the free-stream values equal to one.

The next input to be included in the example problem is incorporation of the values of $(T_{0_\infty} - T_\infty)$ for each second. As already explained in the preceding chapters, the quantity $(T_{0_\infty} - T_\infty)$ plotted against V_∞ gives a single curve for all altitudes up to 370,000 ft. For the actual case, Table A.8 (Appendix 1) needs to be used to get the values of $(T_{0_\infty} - T_\infty)$ for each instant of the flight based on the value of local free-stream velocity V_∞. But for the example problem, the values of $(T_{0_\infty} - T_\infty)$ are given and are shown tabulated in Table 5.1. The data in the table are tabulated for every 2 seconds.

Table 5.1 Velocity and temperature parameters for the trajectory of Figure 5.1 [1].

T sec	V_∞ (ft/sec)	$(T_{0_\infty} - T_\infty)$
0	0	0
2	800	53
4	1600	210
6	1900	300
8	1700	240
10	1500	190
12	3000	700
14	4500	1500
16	5100	1900
18	4800	1700
20	4500	1500
22	6729	3150
24	8958	5550
26	11187	8200
28	13416	11000
30	15645	13750

The next and the final input to be included in the example problem is the instantaneous specific heat c of the skin, which is a function of the temperature. Therefore, it is necessary to have the tabulated values of c for a wide range of temperatures. Table 5.2 contains the values of specific heat for non-oxidized Inconel from 460^0 R to 2060^0 R.

Table 5.2 Specific heat for Nonoxidized Inconel [1].

T (^{0} R)	c (Btu/lb-^{0} R)
460	0.1032
560	0.1065
660	01095
760	0.1130
860	0.1161
960	0.1195
1060	0.1213
1160	0.1240
1260	0.1265
1360	0.1284
1395	0.1289
1460	0.1361
1560	0.1375
1660	0.1396
1760	0.1419
1860	0.1449
1960	0.1475
2060	0.1505

5.3 Discussion

Some small changes were made in the SIMULINK® model to include all the inputs discussed above. Since the ratio of the local free-stream values to the free-stream values is equal to one, and the local free-stream values are already given, the *Free Stream Values* blocks in all the step blocks were deleted. The local free-stream values ρ_0, T_0

and M_0 are directly fed into the *Reynolds Number* block using three *From* file blocks in SIMULINK®. The details of the subsystem *Reynolds Number* block are shown in Figure 5.2

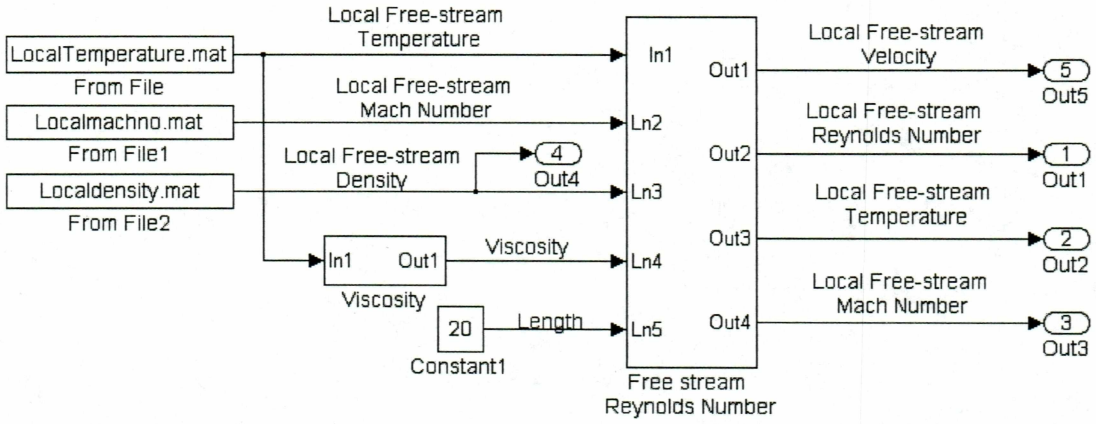

Figure 5.2 SIMULINK® model of the *Reynolds Number* block in the example problem.

To include the values of $(T_{0_\infty} - T_\infty)$ from Table 5.2 in the SIMULINK® model the tabulated data of the *Temperature Difference Table* block were replaced by a *From File* block (Temperature difference.mat). The constant input values (thickness t_s = 0.000417 ft; w = 530 lb/ft^3; and emissivity, ε = 0.9) and the instantaneous specific heat (c) of the skin were updated in the *Constant Values* block and *Specific Heat* look-up table.

Once all the inputs are fed into the SIMULINK® model, the model is run for 30 seconds with a time interval of 1 second.

6 Simulation and Results

6.1 Introduction

In Chapter 4, a MATLAB™ SIMULINK® model was developed to calculate the surface temperature at a particular point on the nose cone. The model is first tested using a solved problem from Truitt [1].

6.2 Results for Example Problem

The example missile is assumed to be a simple ogival body, 40 ft in length, with the proposed flight trajectory shown in Figure 5.1. The skin material is taken to be nonoxidized Inconel; thickness, t_s = 0.000417 ft; specific weight, w = 530 lb/ft^2; and emissivity ε = 0.9. In the present problem, the skin temperature is to be predicted for a point located 20 ft back from the nose cone tip. For simplicity it is assumed that at this location on the ogive, the local pressure coefficient is zero, so that the local conditions are same as those of the free-stream. In experimental missile test programs, often the free-air temperature, pressures, etc., at altitude are measured by a radiosonde at the launching area prior to the flight. For preliminary design these detailed data are usually not available beforehand. However it is a simple matter to prepare these data, using standard atmospheric tables in conjunction with the proposed flight trajectory (Figure 5.1).

The inputs for the example problem are not the same as the ones for the actual problem. The changes made to the model are discussed in detail in Chapter 3. The simulation is run for a time period of 30 seconds with a time step of 1 second. The inputs to the example problem include free-stream density ρ_0, free-stream temperature T_0, Mach number M_0 and the value of $(T_{0_\infty} - T_\infty)$ for each second. The values of the first three parameters are given in Table A.7 (Appendix 1) and the last parameter is given in Table A.8 (Appendix 1).

The first step in the simulation is to obtain the different binary data files used by the *Input Parameters* block for the various cases. These data are obtained from the "time vs. altitude.xls" file using the m-file "example_input_file". When the m-file is run, it prompts the user with the maximum time interval possible and asks for the required time period for the simulation. Based on the time period given, all the required parameters will be generated and fed into the model using the *from* block.

Figure 6.1 V shows the variation of all the four inputs (free-stream temperature, free-stream density, free-stream Mach number and stagnation temperature rise) with time. The simulation is run by selecting the run button in the SIMULINK® model window.

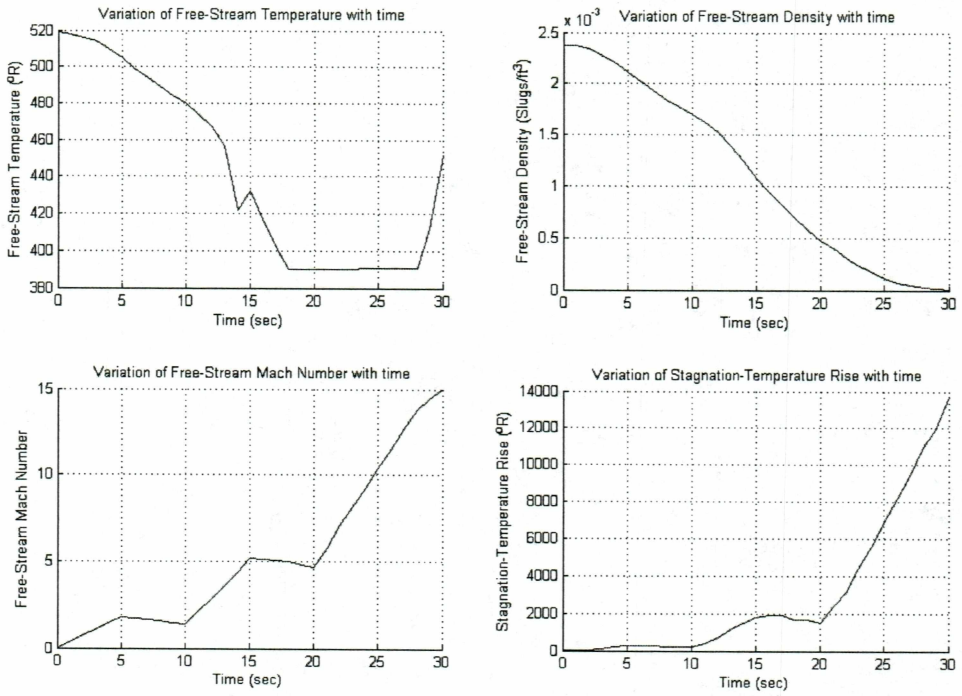

Figure 6.1 Variations of different inputs with time for given trajectory.

In Figure 6.2, the Reynolds numbers obtained from the SIMULINK® model for a time period of 30 seconds with a time interval of 2 seconds are shown. It also shows a comparison of Reynolds number obtained from the SIMULINK® model with that of the textbook [1].

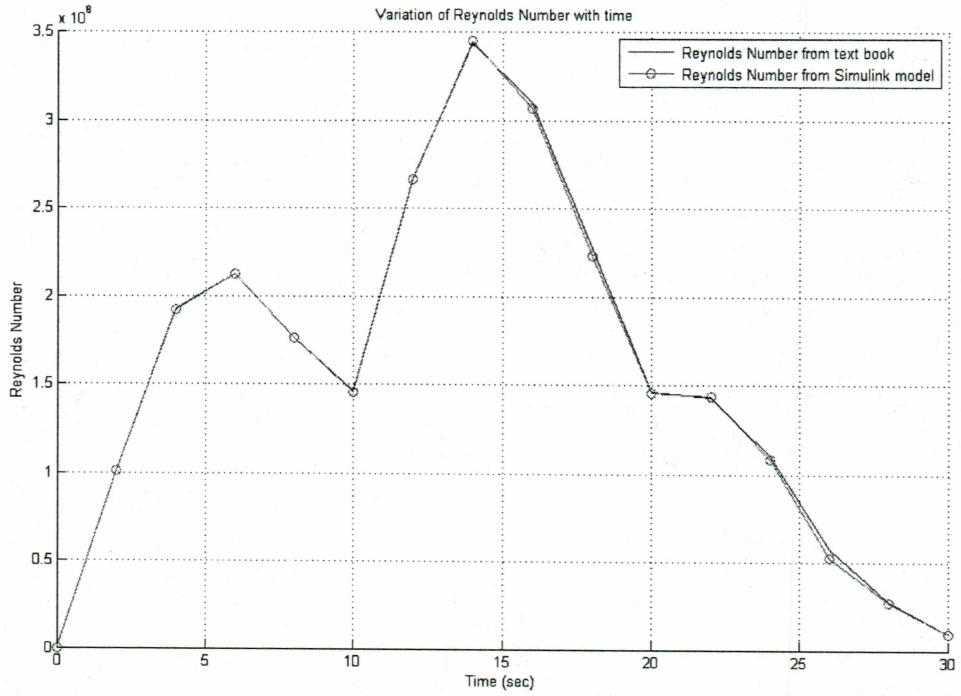

Figure 6.2 Comparison of Reynolds number for given trajectory from the SIMULINK® model and textbook [1] .

In Figure 6.3, the variation of the skin-friction coefficient obtained from the SIMULINK® model for a time period of 30 seconds with a time interval of 2 seconds is shown. We can see that the laminar skin-friction coefficient is zero throughout the simulation. This is due to the fact that during the whole flight, the missile travels in the turbulent flow regime.

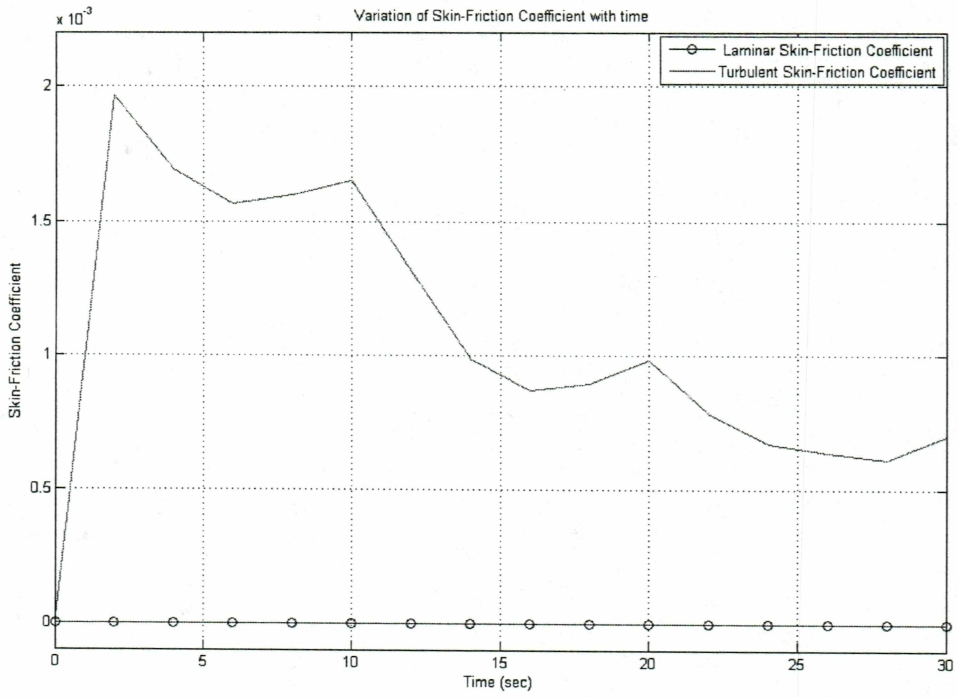

Figure 6.3 Variation of skin-friction coefficient with time for given trajectory.

In Figure 6.4, the variation of the skin temperature obtained from the SIMULINK® model for a time period of 30 seconds with a time interval of 2 seconds is shown. It also shows the comparison of results for skin temperature as obtained from the SIMULINK® model with those of the textbook [1].

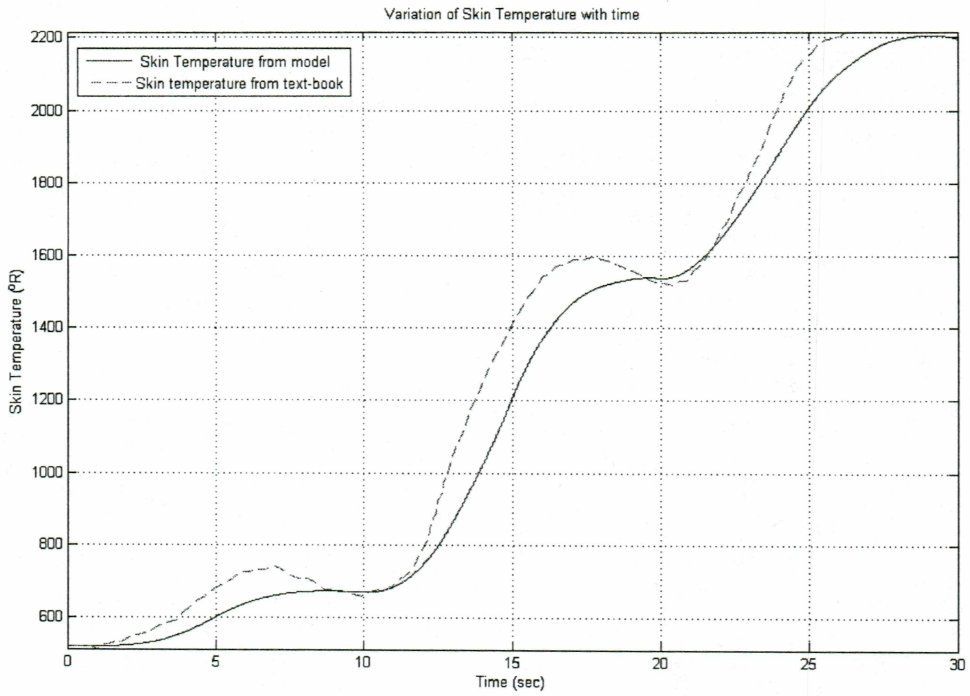

Figure 6.4 Variation of skin temperature with time for given trajectory.

6.3 Results for Student Rocket Project-5

The SRP-5 nose cone is assumed to be a simple ogival body, 6.5 ft in length, with the proposed flight trajectory shown in Figure 6.5. The skin material is taken to be fiberglass/high temperature resin composite; thickness, t_s = 0.010416 ft; specific weight, w = 150.3 lb/ft^2; and emissivity, ε = 0.8. In the present problem, the skin temperature is to be predicted for a point located 5.5 ft back of the nose cone tip. The inputs to this problem include time, altitude and the velocity of the rocket. The simulation is run for a time period of 298 seconds with a time interval of 0.001 seconds. The results from the SIMULINK® model are then compared with the results obtained from NSROC. The computer program used by NSROC computes the temperature time histories of thick wall bodies using Van Driest, Sibulkin, and Kemp-Riddell equations for heat input. The general method assumes that the body can be broken into a number of individual blocks, and the temperature history for each block can be determined. The process was done

assuming one dimensional heat transfer; that is, there are no appreciable effects due to the gradients which exist in the longitudinal direction

The first step in the simulation process is to obtain the different binary data files used by the *Input Parameters* block for the various cases. These data are obtained from a "time vs. altitute.xls" file using the m-file "input_file". When the m-file is run, it prompts the user with the maximum time interval possible and asks for the required time period for the simulation. Based on the time period given, all the required parameters will be generated and fed into the model using the *from* block.

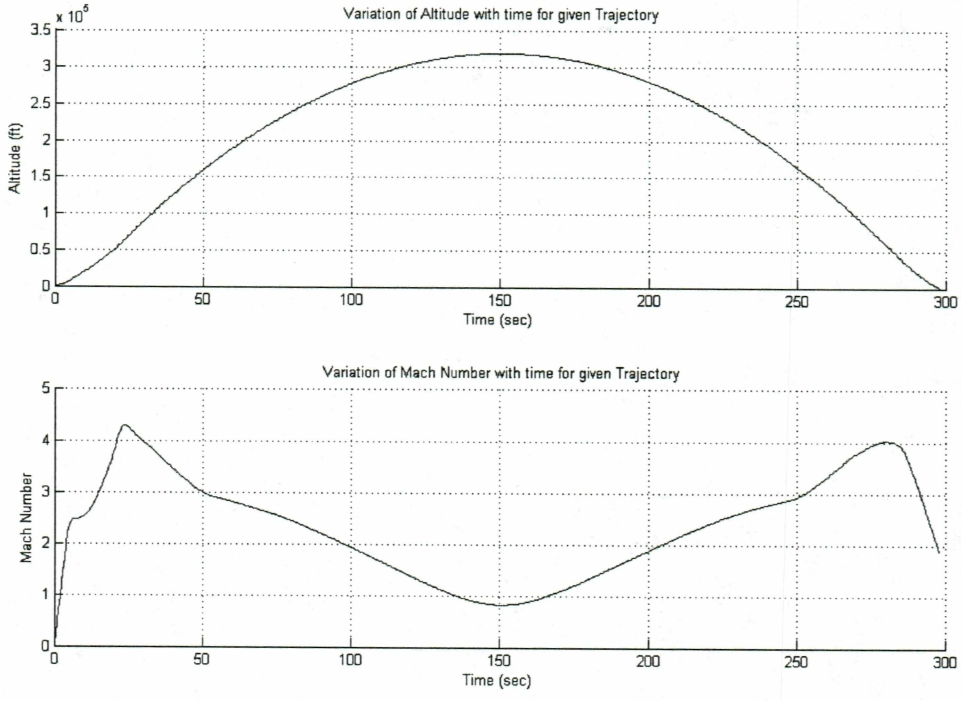

Figure 6.5 Variation of altitude and Mach number for SRP-5 rocket trajectory.

Figure 6.6 shows the variation of the free-stream values (free-stream density, free-stream temperature and free-stream Mach number) obtained from the SIMULINK® model for a time period of 298 seconds with a time interval of 0.001 seconds.

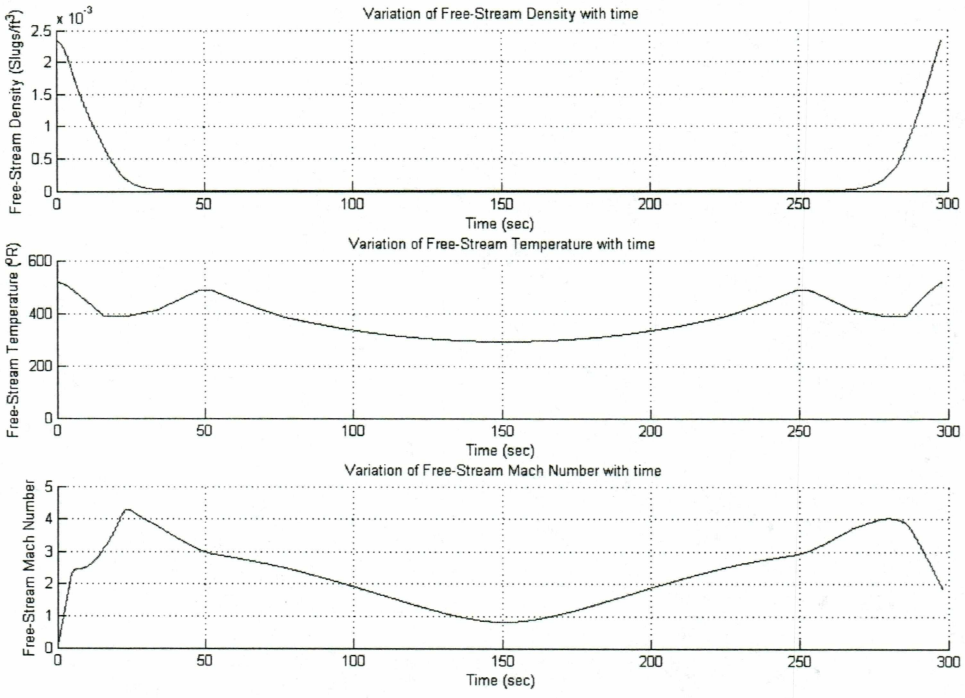

Figure 6.6 Variation of free-stream values with time.

Figure 6.7 shows the variation of the local free-stream values (free-stream density, free-stream temperature and free-stream Mach number) obtained from the SIMULINK® model for a time period of 298 sec with a time interval of 0.001 sec. The supersonic tables used for the calculation of local free-stream values were given for a minimum Mach number of 1.5. To incorporate the values between 0 to 1.5 Mach numbers, an extra row of data is included for a Mach number of zero. The look-up tables used in the SIMULINK® model use cubic spline interpolation for all the data between the points.

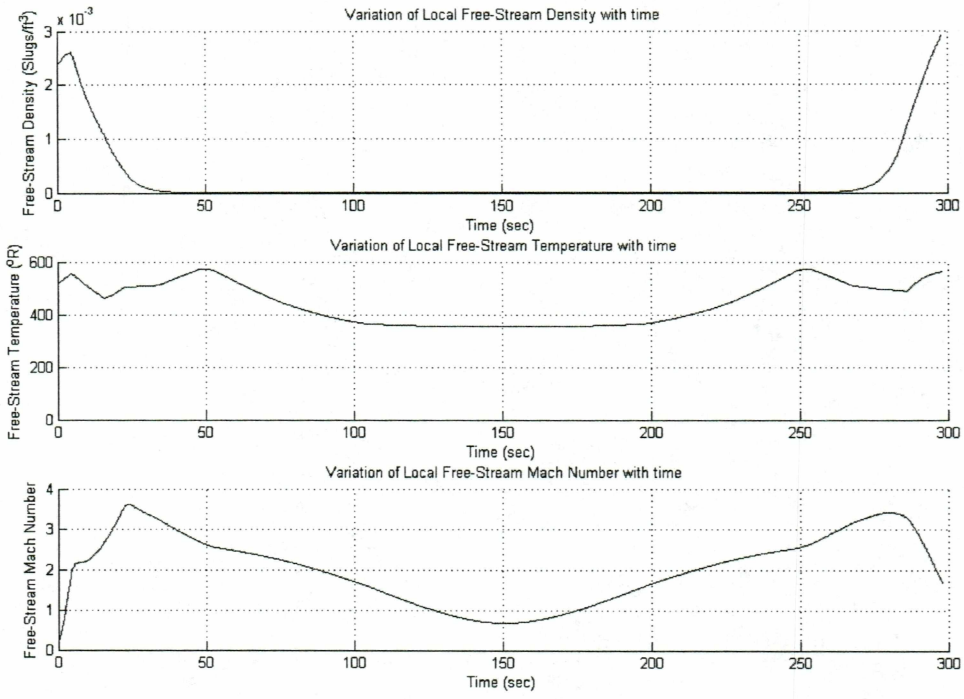

Figure 6.7 Variation of local free-stream values with time.

Figure 6.8 shows the variation of the Reynolds number obtained from the SIMULINK® model for a time period of 200 sec with a time interval of 0.001 seconds. It also shows a comparison of the results of Reynolds number obtained from the SIMULINK® model with the data obtained from NSROC. The difference between the two profiles is due to the fact that the SIMULINK® model uses the formulas given in Table A.1 to predict the atmospheric properties. So the atmospheric model included in the SIMULINK® model uses linear extrapolation for any data required between 232,940 ft (71 km) and apogee which was 318,766 ft (97 km) for this trajectory (If the block input is less than the first or greater than the last input vector element, the block extrapolates using the first two or last two points.).

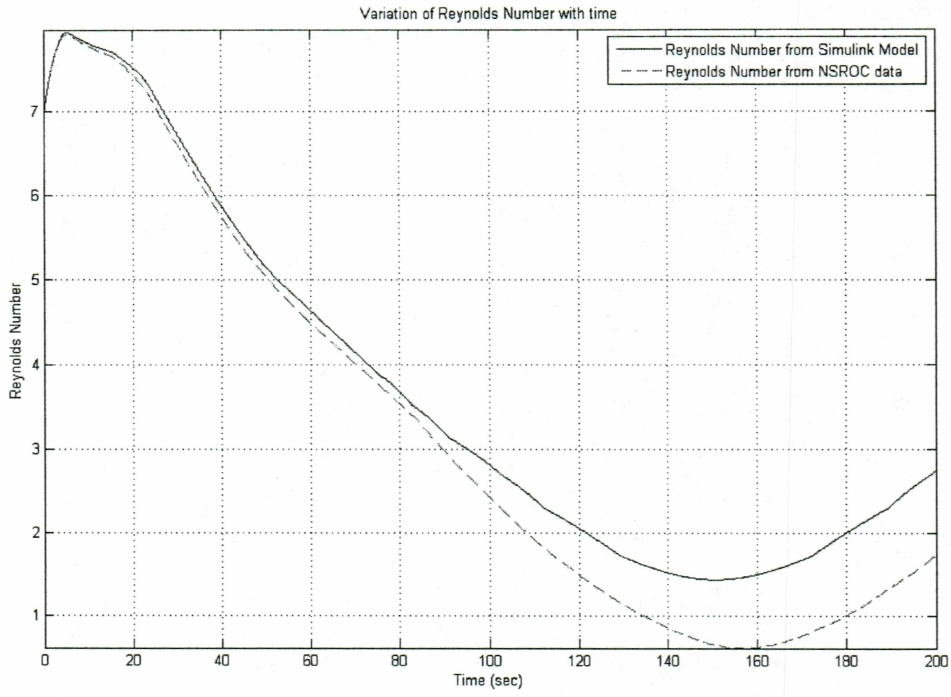

Figure 6.8 Variation of Reynolds number with time.

Figure 6.9 shows the variation of the skin-friction coefficient obtained from the SIMULINK® model for a time period of 298 seconds with a time interval of 0.001 seconds. In this case a transition Reynolds number of 2×10^6 was used. We can see that the laminar skin-friction coefficient is more prominent thought most of the trajectory.

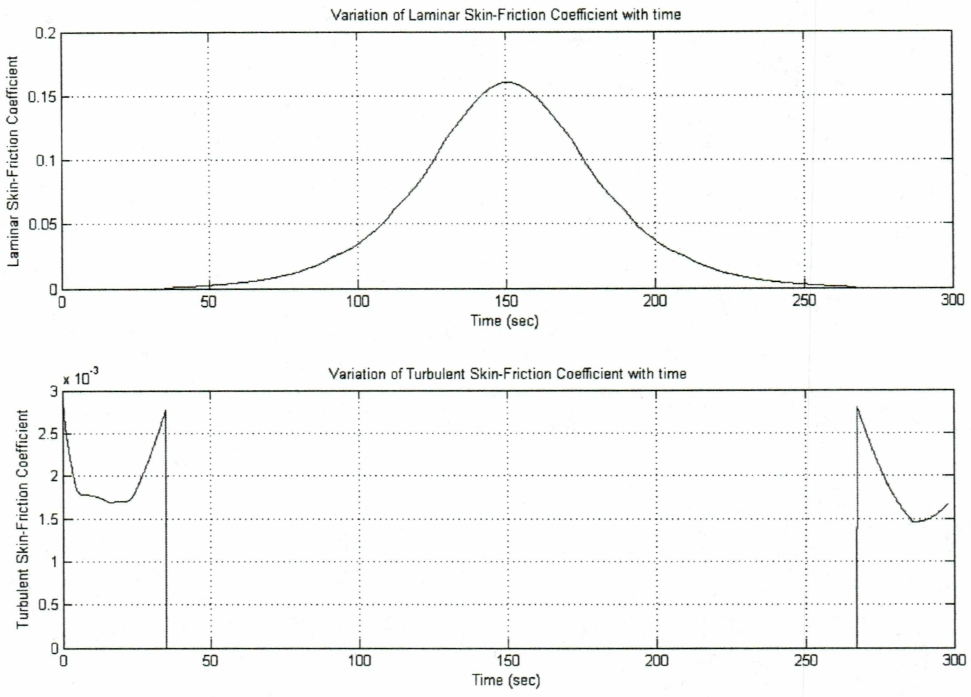

Figure 6.9 Variation of skin-friction coefficient with time.

In Figure 6.10, the variation of the frictional and radiation heat loss parts of Eqs. 2.19 and 2.23, obtained from the SIMULINK® model for a time period of 298 seconds with a time interval of 0.001 seconds, are shown. We can see that the frictional part becomes almost zero between 35 seconds to 265 seconds. This is due to the fact that the local free-stream density term in the Eqs. 2.19 and 2.23 (as shown in first subplot of Figure 6.7) becomes almost negligible during this time interval.

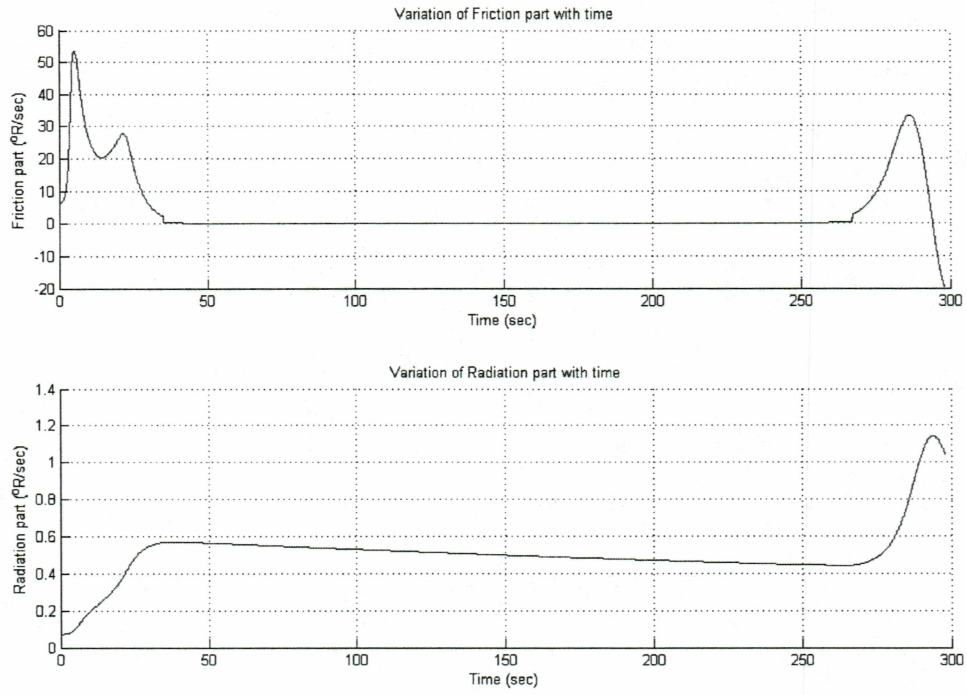

Figure 6.10 Variation of friction and radiation terms with time for given trajectory.

In Figure 6.11, the variation of adiabatic wall temperature obtained from the SIMULINK® model for a time period of 200 seconds with a time interval of 0.001 seconds is shown. We can observe that there is sudden change in the profile at around 35 seconds. This is due to the fact that Eq. 2.13 was used in the calculation of adiabatic wall temperature, and that the recovery factor value changes from $Pr^{1/3}$ to $Pr^{1/2}$ as the flow regime changes from turbulent to laminar.

It also shows the comparison of results for adiabatic wall temperatures as obtained from the SIMULINK® model with the adiabatic wall temperature data obtained from NSROC. The difference between the two profiles is due to the fact that the atmospheric model used in the calculation of free-stream temperature, T_{∞}, is based on formulas given in the Table A.1. The SIMULINK® model uses linear extrapolation for any data required between 232,940 ft (71 km) and apogee, which was 318766.4 ft (97.16 km) for this

trajectory. One more term affecting the differences in the profiles is the values of the Prandtl number, which depend on the wall temperature from the last time step.

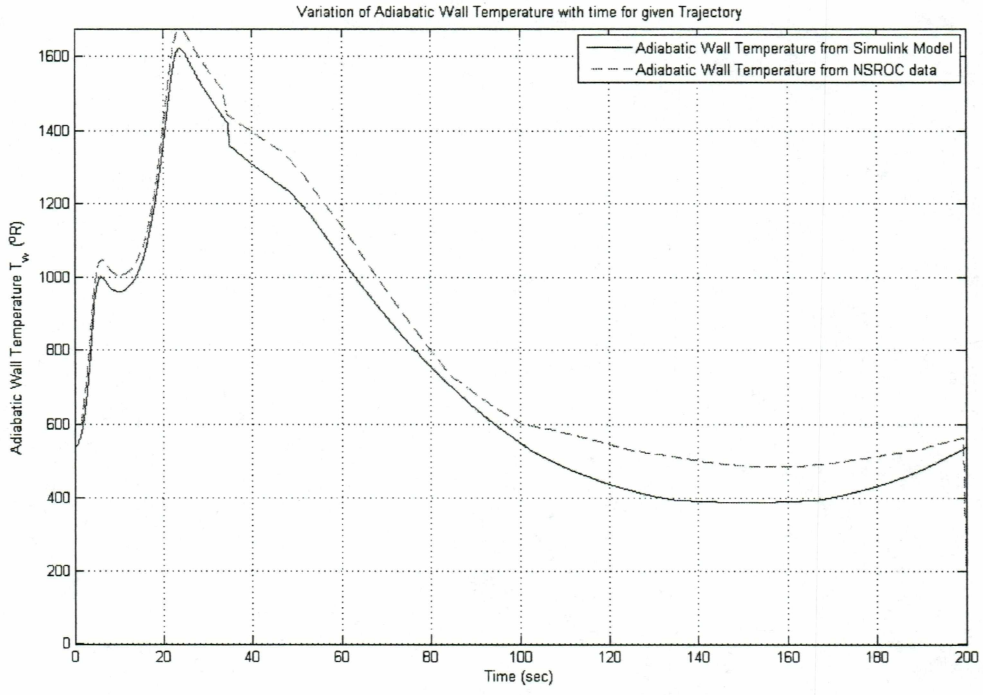

Figure 6.11 Variation of adiabatic wall temperature with time.

In Figure 6.12, the variation of wall temperature is shown for the SRP-5 nose cone at different locations (6" and 66" from the nose tip), as obtained from the SIMULINK® model for a time period of 298 seconds with a time interval of 0.001. We can observe from the figure that the skin temperature at 6" is always greater than the skin temperature at 66" from the nose tip. This is due to the fact that the skin temperature decreases as we move away from the nose tip (stagnation point).

We can also observe that there is an increase in skin temperature for first 35 seconds, and then a gradual decrease until 265 seconds, and then there is an additional increase in skin temperature. This is due to the fact that the first part (friction heat transfer) of the Eqs. 2.13 and 2.19 is negligible between 35 and 265 seconds. During this

time interval, the only prominent factor in Eqs. 2.13 and 2.19 is the second part (radiation heat loss). So even though there is an increase in the adiabatic wall temperature after 35 seconds, the only heat transfer is due to radiation (negative part in Eqs. 2.13 and 2.19), which leads to a gradual decrease in wall temperature.

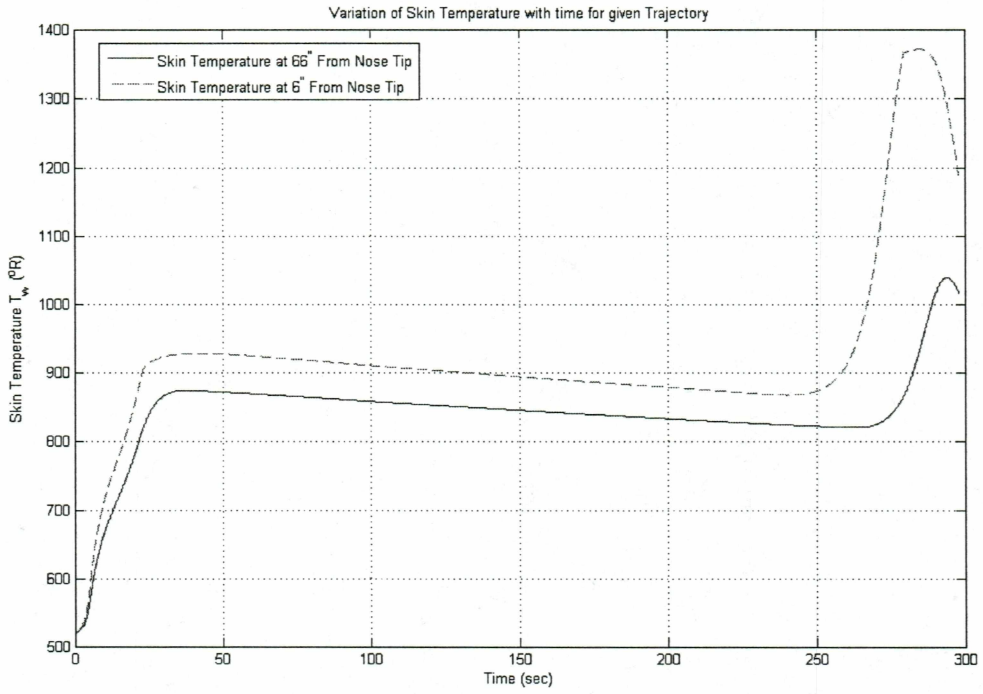

Figure 6.12 Variation of skin temperature at different locations of nose cone with time.

In Figure 6.13, the variation of the skin temperature obtained from the SIMULINK® model for a time period of 200 seconds with a time interval of 0.001 seconds is shown. As in Figure 6.12, we can observe that there is an increase in skin temperature for first 35 seconds and then there is a gradual decrease. Figure 6.13 also shows the comparison of results for skin temperature obtained from the SIMULINK® model with the average skin temperature data obtained from NSROC. The reasons for the difference between the two profiles are same as those explained in the cases of the Reynolds number and adiabatic wall temperature plots. One more reason is that only one

block of skin material is considered in the SIMULINK® model, whereas in the case of the NSROC data, the total thickness of the skin material is divided into 5 layers. Figure 6.13 also shows the variation of the skin temperature of block-1 from NSROC data. We can observe that the temperature of this layer is very high when compared to the average skin temperature from NSROC data and the skin temperature from the SIMULINK® model. Because of the high skin temperature in the NSROC data, overall heat transfer to the skin is reduced during the first portion of the flight. As a consequence, the average skin temperature given by the NSROC data is lower than that produced by the SIMULINK® model.

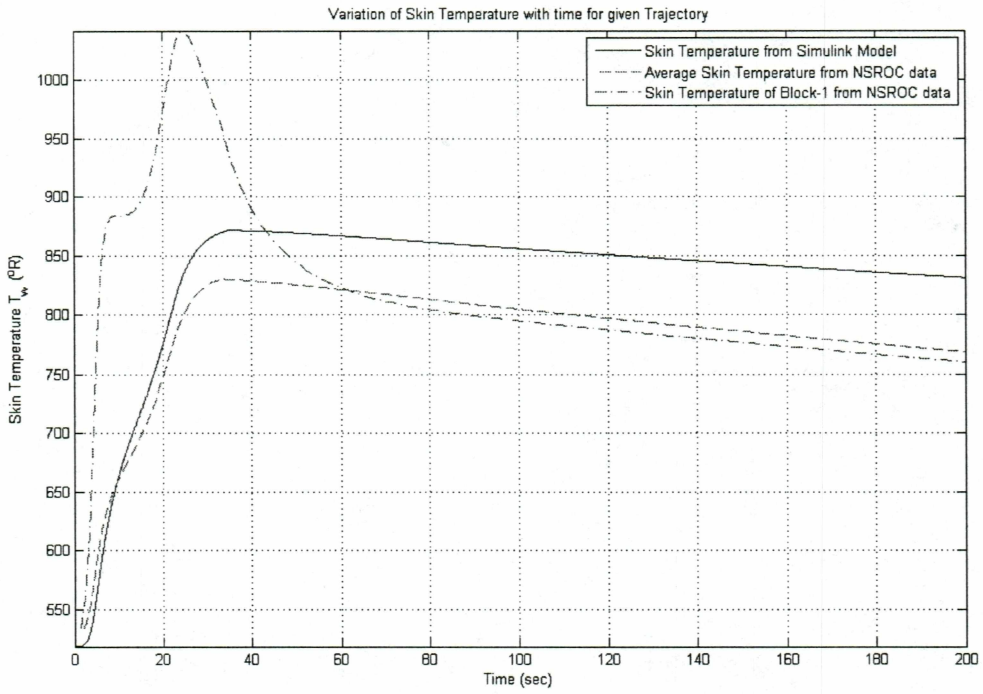

Figure 6.13 Variation of skin temperature with time.

7 Conclusion and Future Work

7.1 Conclusions

The present thesis consists of two parts. First, a general method for determining the skin temperature of bodies during high-speed flight was developed. The governing differential equation was presented for this purpose, giving the fundamental relationship between the skin temperature and flight history. The determination of all the required parameters in the equation was discussed, and the Runge-Kutta numerical method of integration was used to obtain the solution.

The second part of the thesis consisted of implementing the above equations in SIMULINK® to predict skin temperature for the given trajectory. The mathematical models of these individual components (Free-stream Values, Reynolds number, laminar and turbulent skin friction coefficient) were compiled and tested in SIMULINK®. The assembly was then tested by solving one of the example problems given in reference [1]. The simulation results of all the subsystems for the given set of inputs show all the components work. The SIMULINK® model is used to predict the variation of the skin temperature for SRP-5 flight trajectory. The simulation results also show comparison of the different subsystems with the data provided by NSROC.

The selection of SIMULINK® as the computation tool, and the selection of the program structure currently used, is based on the user friendliness, potential for practical applications, and potential for further development. This program is module (subsystems) based and the modules are individually tested and assembled.

For the example problem, the computation time for a 30 second simulation was 9.67 seconds. For the SRP-5 flight trajectory, the computation time for a 298 second

simulation was 35.56 seconds. The computer used for this simulation has a 1.19 GHz processor and a RAM of 512 MB.

7.2 Future Work

In this study, the approximations in the blocks used in the model may cause accumulated errors in the computation results and the use of a large number of equations for system simulation may cause the computation to be inefficient. One possible method for improving computational efficiency and avoiding accumulated computation errors is to apply in-situ measurements, which measure some of the parameters listed in the system equations, such as local free-stream values. Some of the measured data may be used to adjust the computation errors and/or as the inputs of the simulation program to reduce the computation time.

In the present model, the time step remains constant irrespective of the variability in events. By using a variable time step related to variability in the events optimizes the computation.

The accuracy of the current SIMULINK® model could also be improved by implementing a multi-layer skin model similar to the one used in the NSROC calculations. As discussed in Chapter 6, one of the reasons for the different skin temperature predictions had to do with the use of a single skin layer in the current simulation.

Improvements could also be made by optimizing the mathematical and SIMULINK® model by implementing modifications in the model, using s-function blocks, reducing the computational time, and validating the models.

References

1. Truitt, R. W., *Fundamentals of Aerodynamic Heating*, The Glenn L. Martin Co., March, 1957.
2. Van Driest, E. R., *The Problem of Aerodynamic Heating*, Aeronautical Engineering Review, October, 1956.
3. Pohlhausen, E., *Der Warmeaustausch Zwischen frestem Korper Und Flussigkeiten Mit Kliiner Reibung Und Kleiner Warmeleitung,* Z. F. Angew. Math. U. Mech., Vol. 1, No. 2, 1921, pp. 115-121.
4. Crocco, L., *Transmission of Heat from a Flat Plate to a Fluid Flowing at a High Velocity,* National Advisory Committee for Aeronautics, TM, No. 690, 1932.
5. Perkins, J. N., *The Effect of Heat Insulation on the Cooling Requirements of the Internal Structure of High-Speed Vehicles,* Thesis, Virginia Polytechnic Institute, April 29, 1958.
6. Von Karman, T., *The Problem of Resistance in Compressible Fluids,* Royal Academy of Italy, Rome, 1936.
7. Von Karman, T., and Tsien, H. S., *Boundary Layer in Compressible Fluids,* Journal of Aeronautical. Sciences, Vol. 5, No. 6, April 1938, pp.227-232.
8. Huston, W. B., Warfield, C. N., and Stone, A. Z., *A Study of Skin Temperature of Conical Bodies in Supersonic Flight,* National Advisory Committee for Aeronautics, TN 1724, October, 1948.
9. Botzmann, L., *Wiedemannns Annale,* Vol. 22 (p. 291), 1884.
10. Lo, H., *Determination of Transient Skin Temperature of Conical Bodies during Short-Time, High-Speed Flight,* National Advisory Committee for Aeronautics TN 1725, October, 1948.
11. Van Driest, E. R., *Turbulent Boundary Layer on a Cone in a Supersonic Flow at Zero Angle of Attack,* Journal of Aeronautical Sciences, Vol.19, No.1, P.55, 1952.

12. Van Driest, E. R., *The Turbulent Boundary Layer with Variable Prandtl Number,* 50 Jahre Grenzschichtforschung, pp.257-271, Friedr. Vieweg and Sohn, Verlag, Braunschung.

13. Anderson, J. D., Jr., *Hypersonic and High Temperature Gas Dynamic,s* McGraw-Hill series in Aeronautical and Aerospace Engineering, 1989.

14. Wood, G. P., *Calculation of Surface Temperature in Steady Supersonic Flight,* National Advisory Committee for Aeronautics, TN 1114, 1946.

15. White, F. M., *Viscous Fluid Flow,* McGraw-Hill Book Co., 2nd ed., 1991.

16. Anderson J. D., Jr., *Modern Compressible Flow with Historical Perspective,* McGraw-Hill series in mechanical engineering, 3rd ed., 2003.

17. Bertin, J. J., and Smith M. L., *Aerodynamics for Engineers,* Prentice-Hall, Inc., 3rd ed., 1998.

18. Anderson, J. D., Jr., *Fundamentals of Aerodynamics,* McGraw-Hill series in Aeronautical and Aerospace Engineering, 3rd ed., 2001.

19. Saad, M. A., *Compressible Fluid Flow,* Prentice-Hall, Inc., 2nd ed., 1993.

20. Shapiro, A. H., *The Dynamics and Thermodynamics of Compressible Fluid Flow,* The Ronald Press Company, Vol.2, 1954.

21. Keenan, J. H., and Kaye, J., *Thermodynamic Properties of Air Including Polytropic Functions,* John Wiley and Sons, New York, 1945.

22. Fujii K., and Watanabe S., *Aerodynamic Heating Measurements on Nose and Elevon of Hypersonic Flight Experiment Vehicle*, Journal of Spacecraft and Rockets, Vol.38, No.1, Jan-Feb 2001.

23. Fujii, K., and Inoue Y., *Aerodynamic Heating Measurement on Afterbody of Hypersonic Flight Experiment,* Journal of Spacecraft and Rockets, Vol.35, No.6, Nov-Dec 1998.

24. James, R., Hayes, and Richard D. Neumann., *Introduction to the Aerodynamic Heating Analysis of Supersonic Missiles,* American Institute of Aeronautical Engineering, 1986.

25. Riley, C. J., and Dejarnette, F. R., *An Engineering Aerodynamic Heating Method for Hypersonic Flow,* American Institute of Aeronautical Engineering, 1992.

26. Maitra, S. N., *Aerodynamic Heating of Ballistic Missile including the Effect of Gravity,* Sadhana-Academy Processing in Engineering, Vol.25, Part 5, October, 2000.

27. Joseph, L., and Sims, *Tables for Supersonic Flow around Right Circular Cones at zero angle of attack,* National Aeronautices and Space Administration, 1964.

28. http://scipp.ucsc.edu/outreach/balloon/index.html, [last updated 04/05]

29. http://www.aerospaceweb.org/question/atmosphere/q0049.shtml, [last updated 04/05]

Appendix 1: Tables

Table A.1. Standard atmospheric data calculation formulas

S.No	Altitudes Up to:	English Unite Temperature (R) Density (Slug/ft3) Pressure (lb/ft2)	Metric units Temperature (K) Density (Kg/m3) Pressure (N/m2)
h is measured in:		Feet	Meters
1	11 km	$T = T0\ (1-h/145442\ ft)$ $r = r0\ (1-h/145442\ ft)^{4.255876}$ $P = P0\ (1-h/145442\ ft)^{5.255876}$	$T = T0\ (1-h/44329\ m)$ $r = r0\ (1-h/44329\ m)^{4.255876}$ $P = P0\ (1-h/44329\ m)^{5.255876}$
2	20 km	$T = T0\ (0.751865)$ $r = r0\ (0.297076)\ e^{((36089-h)/20806)}$ $P = P0\ (0.223361)\ e^{((.36089-h)/20806)}$	$T = T0\ (0.751865)$ $r = r0\ (0.297076)\ e^{((10999-h)/6341.4)}$ $P = P0\ (0.223361)\ e^{((10999-h)/6341.4)}$
3	32 km	$T = T0\ (0.682457 + h/945374)$ $r = r0\ (0.978261 + h/659515)^{-35.16319}$ $P = P0\ (0.988626 + h/652600)^{-34.16319)}$	$T = T0\ (0.682457 + h/288136)$ $r = r0\ (0.978261 + h/201010)^{-35.16319}$ $P = P0\ (0.988626 + h/198903)^{-34.16319)}$
4	47 km	$T = T0\ (0.482561 + h/337634)$ $r = r0\ (0.857003 + h/190115)^{-13.20114}$ $P = P0\ (0.898309 + h/181373)^{-12.20114}$	$T = T0\ (0.482561 + h/102906)$ $r = r0\ (0.857003 + h/57944)^{-13.20114}$ $P = P0\ (0.898309 + h/55280)^{-12.20114}$
5	51 km	$T = T0\ (0.939268)$ $r = r0\ (0.00116533)\ e^{((154200-h)/25992)}$ $P = P0\ (0.00109456)\ e^{((154200-h)/25992)}$	$T = T0\ (0.939268)$ $r = r0\ (0.00116533)\ e^{((46998-h)/7922)}$ $P = P0\ (0.00109456)\ e^{((46998-h)/7922)}$

TableA.1. (Continued)

6	71 km	$T = T0\ (1.434843 - h/337634)$ $r = r0\ (0.79899 - h/606330)^{11.20114}$ $P = P0\ (0.838263 - h/577922)^{12.20114}$	$T = T0\ (1.434843 - h/102906)$ $r = r0\ (0.79899 - h/184800)^{11.20114}$ $P = P0\ (0.838263 - h/176142)^{12.20114}$

Table A. 2. Values of P_s / P_∞ for each cone angle as a function of nominal free-stream Mach number

θ_s / M_∞	2.5	5.0	7.5	10	12.5	15
1.5	1.0194326	1.0624668	1.1218836	1.1949823	1.2805338	1.3780493
1.75	1.0245272	1.0778796	1.1509820	1.2406790	1.3455754	1.4650276
2.0	1.0302014	1.0950480	1.1836274	1.2924832	1.4202392	1.5662549
2.5	1.0430054	1.1338127	1.2579479	1.4118223	1.5943908	1.8051501
3.0	1.0575531	1.1779135	1.3434709	1.5510936	1.8002508	2.0905385
3.5	1.0736800	1.2270211	1.4399168	1.7101605	2.0377458	2.4222429
4.0	1.0912720	1.2809867	1.542920	1.8892065	2.3071757	2.8006264
4.5	1.1102609	1.3397531	1.6656866	2.0884875	2.6089172	3.2261054
5.0	1.1305848	1.4033150	1.7952468	2.3082460	2.9432816	3.6990542
6.0	1.1750571	1.5449088	2.0883718	2.8100784	3.7110158	4.7885278
7.0	1.2244683	1.7060582	2.4276150	3.3961384	4.6121063	6.0708563
8.0	1.2786974	1.8871344	2.8137638	4.0675451	5.6477433	7.5471315
10.0	1.4015141	2.3102688	3.7291669	5.6691937	8.1254669	11.084206
12.0	1.5435569	2.8164933	4.8380961	7.6189879	11.147954	15.402823
15.0	1.7934152	3.7349358	6.8688796	11.200599	16.706375	23.3487786
20.0	2.3107823	5.6980529	11.241661	18.928672	28.708667	40.511555

Table A.3. Values of ρ_s / ρ_∞ for each cone angle as a function of nominal free-stream Mach number

θ_s / M_∞	2.5	5.0	7.5	10	12.5	15
1.5	1.0138422	1.0442312	1.0856178	1.1356839	1.1931674	1.2573090
1.75	1.0174589	1.0550291	1.1056566	1.1665336	1.2361131	1.3133374
2.0	1.0214806	1.0670052	1.1279661	1.2011081	1.2846332	1.3771650
2.5	1.0305328	1.0938507	1.1781062	1.2792090	1.3946574	1.5220513
3.0	1.0407794	1.1240743	1.2347385	1.3677168	1.5191742	1.6849445
3.5	1.0520914	1.1573491	1.2972924	1.4654187	1.6556363	1.8612362
4.0	1.0643759	1.1934727	1.3653425	1.5711823	1.8016154	2.0467434
4.5	1.0775724	1.2323006	1.4384668	1.6838406	1.9547443	2.2376305
5.0	1.0916254	1.2737154	1.5162344	1.8021900	2.1127395	2.4304985
6.0	1.121267	1.3638529	1.6837852	2.0512090	2.4351514	2.8111096
7.0	1.1556291	1.4629538	1.8640213	2.3091981	2.7547485	3.1716000
8.0	1.1919497	1.5699958	2.0529446	2.5683901	3.0613975	3.5023937
10.0	1.2725510	1.8032648	2.4421857	3.0671848	3.6131848	4.0627948
12.0	1.3630073	2.0542275	2.8266452	3.5166850	4.0707795	4.4961167
15.0	1.5151575	2.4444097	3.3598261	4.0773330	4.5945414	4.9603730
20.0	1.8035356	3.0749176	4.0824004	4.7386323	5.1535214	5.4219261

Table A.4. Values of T_s / T_∞ for each cone angle as a function of nominal free-stream Mach number

θ_s / M_∞	2.5	5.0	7.5	10	12.5	15
1.5	1.0055140	1.0174631	1.0334056	1.0522138	1.0732222	1.0960307
1.75	1.0069473	1.0216586	1.0409941	1.0635604	1.0885536	1.1154998
2.0	1.0085375	1.0262818	1.0493466	1.0760757	1.105601	1.1373037
2.5	1.0121030	1.0365333	1.0677713	1.1036682	1.1432132	1.1859982
3.0	1.0161164	1.0478965	1.0880610	1.1340751	1.1850193	1.2407165
3.5	1.0205197	1.0601996	1.1099400	1.1670116	1.2307931	1.3014162
4.0	1.0252694	1.0733272	1.1332629	1.2024108	1.2806150	1.3683329
4.5	1.0303353	1.0871966	1.1579597	1.2403118	1.3346591	1.4417507
5.0	1.0356893	1.1017492	1.1840166	1.2808006	1.3931114	1.5219323
6.0	1.0471697	1.1327532	1.2402840	1.3699620	1.5239364	1.7034298
7.0	1.0595686	1.1661736	1.3023537	1.4707004	1.6742386	1.9141305
8.0	1.0727780	1.2019996	1.3705990	1.5836944	1.8448252	2.1548496
10.0	1.1013422	1.2811578	1.5269792	1.8483379	2.2488379	2.7282219
12.0	1.1324641	1.3710717	1.7116036	2.1665256	2.7385305	3.4258059
15.0	1.1836493	1.5279500	2.0444152	2.7470405	3.6361355	4.7070625
20.0	1.2812513	1.8530750	2.7536890	3.9945433	5.5706894	7.4718014

Table A.5. Values of Mach number at cone surface for each cone angle as a function of nominal free-stream Mach number.

θ_s / M_∞	2.5	5.0	7.5	10	12.5	15
1.5	1.4866884	1.4579318	1.4197316	1.3748579	1.3248992	1.2707392
1.75	1.7340335	1.7004643	1.658043	1.6064462	1.5513276	1.4925484
2.0	1.9808615	1.9415254	1.8912335	1.8340453	1.7721933	1.7068837
2.5	2.4729472	2.4193976	2.3528628	2.2788768	2.2001554	2.1179422
3.0	2.9627600	2.8913832	2.8048038	2.7101402	2.6103929	2.5067511
3.5	3.4500939	3.3571597	3.2457499	3.1275136	3.0025569	2.8731152
4.0	3.9347700	3.8164543	3.6783916	3.5305680	3.3761469	3.2166972
4.5	4.4166246	4.2690580	4.0994611	3.9189007	3.7307750	3.5374323
5.0	4.8955305	4.7148078	4.5097079	4.2921847	4.0662668	3.8355932
6.0	5.8440686	5.5852474	5.2968787	4.9927832	4.6801702	4.3668118
7.0	6.7796857	6.4269172	6.0384888	5.6318010	5.2204850	4.8178049
8.0	7.7018785	7.2390804	6.7337145	6.2103924	5.6922672	5.1981506
10.0	9.5046400	8.7725147	7.9851813	7.1977580	6.4568340	5.7867581
12.0	11.250395	10.182053	9.0582962	7.9858490	7.0291308	6.2043028
15.0	13.759139	12.063489	10.368285	8.8727901	7.634201	6.6228697
20.0	17.637850	14.613515	11.91918	9.8177450	8.2281047	7.0145241

Table A.6. Prandtl number data

Temperature In Deg-R	Prandtl Number
400	.73
450	.72
500	0.71
550	0.70
600	0.70
650	0.69
700	0.68
750	0.68
800	0.68
900	0.67
1000	0.66
1100	0.66
1200	0.66
1300	0.66
1400	0.65

Table A.7. Tabulated flight trajectory data

t sec	ρ_0 slugs/ft^3	a_0 ft/sec	M_0	T_0 ^0R
0	2.38	1117.089	0	519
1	2.37	1117.089	0.358305	518
2	2.34	1113.874	0.717905	516
3	2.28	1111.99	1.078938	514
4	2.21	1107.116	1.444969	510
5	2.11	1101.101	1.816009	505
6	2.02	1095.019	1.735029	499
7	1.93	1089.992	1.650964	494
8	1.84	1082.932	1.570014	489
9	1.77	1078.938	1.482917	484
10	1.70	1074.048	1.396932	480
11	1.62	1067.946	2.107006	474
12	1.52	1059.995	2.829992	467
13	1.39	1048.903	3.575007	457
14	1.24	1035.088	4.347993	442
15	1.08	1018.007	5.157005	432
16	0.94	1000.999	5.094997	417
17	0.81	984.0813	5.030006	402
18	0.69	967.986	4.958998	390
19	0.57	967.986	4.804004	390
20	0.48	967.986	4.649004	390
21	0.40	967.986	5.79998	390
22	0.31	967.986	6.951019	390
23	0.23	967.986	8.102991	390
24	0.18	970.8237	9.253999	391

Table A.7. (Continued)

25	0.12	970.8237	10.37298	391
26	0.07	970.8237	11.52225	391
27	0.05	970.8237	12.668	391
28	0.03	970.8237	13.81701	391
29	0.02	1006.952	14.42999	412
30	0.01	1043.114	15	452

Table A.8. Stagnation temperature rise with respect to velocity

V_∞ (ft/sec)	$T_{0_\infty} - T_\infty$ (^{0}R)
0	0
774.56	50
1095.4	100
1341.7	150
1549.5	200
1732.8	250
1898.9	300
2051.9	350
2194.8	400
2329.4	450
2457.2	500
2579.2	550
2809.1	650
3023.9	750
3226.8	850
3420.1	950
3605.1	1050
3783.3	1150
3955.3	1250
4121.9	1350
4283.6	1450
4440.9	1550
4594.1	1650
4743.4	1750

Table A.8. (Continued)

4889.2	1850
5031.7	1950
5171.1	2050
5441.3	2250
5701	2450
5951.4	2650
6193.3	2850
6427.6	3050
6654.8	3250
6875.6	3450
7090.3	3650
7299.5	3850
7503.4	4050
7702.5	4250
7897.3	4450
8087.9	4650
8274.8	4850
8458.3	5050
8638.8	5250
8816.8	5450
8992.7	5650

Table A.9. Specific heat for Nonoxidized Inconel

T ($^{\circ}R$)	c (Btu/lb-$^{\circ}R$)
460	0.1032
560	0.1065
660	0.1095
760	0.1130
860	0.1161
960	0.1195
1060	0.1213
1160	0.1265
1260	0.1284
1360	0.1289
1460	0.1361

Appendix 2: M-file to Generate the Input Parameters for the SIMULINK® Model

```
% PROGRAM TO GENERATE THE INPUT DATA FOR THE SIMULINK CODE

clc;
close all;
clear all;

% READING THE DATA FROM THE EXCEL SHEET

A = xlsread('Altitude data-1','Sheet2');
n = length(A(:,1));

% ASSIGNING THE DATA TO VARIABLES

time = A(:,1)';
Alt = A(:,2)';
Vel = A(:,3)';

disp(  sprintf('\n The Minimum time interval is: %7.4f\n', min(diff(A(:,1))))  )
t = input('Enter the time step :')

aa = t/2;
n = length(time);
time2 = [time(1)];
Alt2 = [Alt(1)];
Vel2 = [Vel(1)];

for i = 1:length(time)-1

   time1 = (time(i):aa:time(i+1));
   Alt1 = (linspace(Alt(i),Alt(i+1),length(time1)));
   Vel1 = (linspace(Vel(i),Vel(i+1),length(time1)));
   time2 = [time2 time1(1,(2:length(time1)))];
   Alt2 = [Alt2 Alt1(1,(2:length(time1)))];
   Vel2 = [Vel2 Vel1(1,(2:length(time1)))];

end

% SAVING THE DATA OF ALL THE VARIABLES FOR THE 1ST TIME STEP
```

```
H = [time2(1,(1:length(time2)-2));Alt2(1,(1:length(time2)-2))];
V = [time2(1,(1:length(time2)-2));Vel2(1,(1:length(time2)-2))];
save Altitude1 H
save Velocity1 V

% SAVING THE DATA OF ALL THE VARIABLES FOR THE 2ND AND 3RD TIME
STEP

H1 = [time2(1,(1:length(time2)-2));Alt2(1,(2:length(time2)-1))];
V1 = [time2(1,(1:length(time2)-2));Vel2(1,(2:length(time2)-1))];
save Altitude2 H1
save Velocity2 V1

% SAVING THE DATA OF ALL THE VARIABLES FOR THE 4TH TIME STEP

H2 = [time2(1,(1:length(time2)-2));Alt2(1,(3:length(time2)))];
V2 = [time2(1,(1:length(time2)-2));Vel2(1,(3:length(time2)))];
save Altitude4 H2
save Velocity4 V2

Stop = V2(1,length(time2)-2)
```